LMEC-Memo-70-5
Limited Distribution

Examination of Four Sodium-Water Reaction Target Tubes

By
W. T. Lee

This document is
PUBLICLY RELEASABLE
H. Kinser
Authorizing Official
Date: 6/12/06

~~NOTICE~~
~~This report contains information of a preliminary nature and was prepared primarily for internal use at the originating installation. It is subject to revision or correction and therefore does not represent a final report. It is passed to the recipient in confidence and should not be abstracted or further disclosed without the approval of the originating installation or DTI Extension, Oak Ridge.~~

LEGAL NOTICE
This report was prepared as an account of work sponsored by the United States Government. Neither the United States nor the United States Atomic Energy Commission, nor any of their employees, nor any of their contractors, subcontractors, or their employees, makes any warranty, express or implied, or assumes any legal liability or responsibility for the accuracy, completeness or usefulness of any information, apparatus, product or process disclosed, or represents that its use would not infringe privately owned rights.

Liquid Metal Engineering Center

Operated for
the U.S. Atomic Energy Commission by Atomics International
A Division of North American Rockwell Corporation

Contract: AT(04-3)-700

Issued: June 26, 1970

Released For Announcement in Energy Research Abstracts. Distribution Limited to Participants in the LMFBR Program. Others request from TIC

~~DISTRIBUTION OF THIS DOCUMENT IS UNLIMITED to AEC Offices and AEC Contractors~~

DISCLAIMER

This report was prepared as an account of work sponsored by an agency of the United States Government. Neither the United States Government nor any agency Thereof, nor any of their employees, makes any warranty, express or implied, or assumes any legal liability or responsibility for the accuracy, completeness, or usefulness of any information, apparatus, product, or process disclosed, or represents that its use would not infringe privately owned rights. Reference herein to any specific commercial product, process, or service by trade name, trademark, manufacturer, or otherwise does not necessarily constitute or imply its endorsement, recommendation, or favoring by the United States Government or any agency thereof. The views and opinions of authors expressed herein do not necessarily state or reflect those of the United States Government or any agency thereof.

DISCLAIMER

Portions of this document may be illegible in electronic image products. Images are produced from the best available original document.

CONTENTS

	Page
Abstract	7
I. Introduction	9
II. Experimental	13
A. Dimensional and Volumetric Measurements	13
B. Heat Treatment	13
C. Metallographic Sample Preparation	17
III. Results	19
A. Extent of Material Wastage	19
B. Metallography of Control (Quenched) Samples	19
1. 2-1/4 Cr - 1 Mo Ferritic Steel	19
2. Incoloy 800	23
3. Type 304 SS	23
C. Examination of Affected Areas in the Target Tubes	30
1. Tube No. 37 (2-1/4 Cr - 1 Mo Ferritic Steel)	30
2. Tube No. 21 (Incoloy 800)	32
3. Tube No. 29A (Type 304 SS)	39
4. Tube No. 15 (2-1/4 Cr - 1 Mo Ferritic Steel)	39
IV. Discussions	47
A. Extent of Wastage	47
B. Metallographic Analysis	54
C. Nature of Damage Caused by Water-Jet Impact and Sodium-Water Reaction	59
D. Possible Wastage Mechanism	60
E. Other Factors Affecting Wastage Rate	60
V. Conclusions	65
References	67

TABLES

1. Compositions of the Exposed Target Tube Materials	10
2. Data Summary for APDA Samples	11
3. Test Matrix	14
4. Dimensions of Impacted Areas for Four Rig 10 Target Tubes	20

CONTENTS

		Page
5.	Volume of Impacted Areas for Four Rig 10 Target Tubes	20
6.	Comparison of LMEC and SRI Measurements on Four APDA Sodium-Water Reaction Target Tubes	48
7.	Variation of Strain Energy with Temperature for Incoloy 800, Type 304 SS, and 2-1/4 Cr - 1 Mo Steel	52
8.	Variation of Ultimate Resilience with Temperature for Incoloy 800, Type 304 SS and 2-1/4 Cr - 1 Mo Ferritic Steel	56

FIGURES

1.	Retort and Sample Holder for the Quenching Experiment	15
2.	Quenching Apparatus with Retort Installed in Furnaces	16
3.	Typical Thermal History for a Batch of Four Specimens (Batch No. 10, 5-min Soak)	18
4.	Microstructures of 2-1/4 Cr - 1 Mo Steel Quenched to 600°F	21
5.	Microstructure of 2-1/4 Cr - 1 Mo Steel Quenched from 1800°F to 600°F in a Helium Environment	21
6.	Microstructure of 2-1/4 Cr - 1 Mo Steel Quenched from Various High Temperatures to 600°F in a Helium Environment (5-min Soak)	22
7.	Effect of Quench Temperature on Average Room Temperature Hardness of 2-1/4 Cr - 1 Mo Steel	24
8.	Microstructure of Incoloy 800 Quenched from Various High Temperatures to 600°F in Helium (5-min Soak)	25
9.	Effect of Quenching Temperature on Room Temperature Hardness of Incoloy 800	27
10.	Microstructure of Type 304 SS Quenched from Various High Temperatures to 600°F in Helium (5-min Soak)	28
11.	Ferritic Steel Tube Section Showing Area of Metal Removal (Wastage) after Steam Impingement in 600°F Sodium	30
12.	Microstructure of Impact Area of 2-1/4 Cr - 1 Mo Steel after Sodium-Water Reaction	31
13.	Decarburized Layer (~ 3 mil thick) on Outside Diameter of Tube No. 37 in Areas away from Impact Cavity	31
14.	Elongated Grains in Areas Adjacent to the Impact Area, Showing Plastic Deformation	32

CONTENTS

		Page
15.	Knoop Hardness (KHN) Variation in Wasted Areas for Tube No. 37 (2-1/4 Cr - 1 Mo Ferritic Steel)	33
16.	Macrograph of Tube No. 21 (Incoloy 800) after Water-Jet Impact, Showing the Impact Indentation	34
17.	Carbide Distribution in Incoloy 800 Exposed to Sodium-Water Reactions	35
18.	Incoloy 800 Exposed to Sodium-Water Reactions, Showing the Elongated Grains in an Area Adjacent to the Impact	37
19.	Microstructure of Incoloy 800 Tube Exposed to Sodium-Water Reactions, Showing Carbide Precipitation and Minor Intergranular Corrosion on Tube Outside Diameter away from Impact	37
20.	Apparent Corrosion or Depletion Layer (~ 0.5 mil) on the Tube Outside Diameter of Tube No. 21 (Incoloy 800)	38
21.	Comparison of the Hardness Indentation on the Depletion Layer and on the Base Material	38
22.	Macrograph of the Impact Area on Tube No. 29A (Type 304 SS)	40
23.	Typical Microstructure of Tube Outside Diameter in Impact Area, Showing Absence of any Corrosion	41
24.	Typical Microstructure of Tube Outside Diameter in Areas away from Impact, Showing Intergranular Corrosion and Surface Pitting	41
25.	Microstructure of Tube Outside Diameter about 3/4 in. away from the Center of Impact, Showing Corrosion and Plastic Deformation Lines	43
26.	Enlarged View of the Microstructure in the Indented Area, Showing Intergranular Corrosion, Plastic Deformation Lines, and Carbide Precipitation	43
27.	Microstructures of Tube Inside Diameter, Showing the Absence of Carbide Precipitation	45
28.	Macrograph of the Impact Area on Tube No. 15 (2-1/4 Cr - 1 Mo Steel)	46
29.	Hot Microhardness Data for Incoloy 800, Type 304 SS, and a Ferritic Steel	50
30.	Effect of Temperature on Tensile Strength of Annealed Incoloy 800, Type 304 SS, and 2-1/4 Cr - 1 Mo Ferritic Steel	51
31.	Variation of Calculated Strain Energy with Temperature for Incoloy 800, Type 304 SS, and 2-1/4 Cr - 1 Mo Ferritic Steel	53
32.	Dependence of Wastage Rate on Strain Energy of Material	55
33.	Variation of Ultimate Resilience with Temperature for Incoloy 800, Type 304 SS, and 2-1/4 Cr - 1 Mo Ferritic Steel	57
34.	Time-Temperature Dependence of $Cr_{23}C_6$ Precipitation in Incoloy 800 with 0.07% C	58

ACKNOWLEDGMENT

The author wishes to acknowledge the technical guidance of Mr. R. K. Wagner; appreciation is extended to Mr. K. L. Adler, Sodium-Water Reaction Program Project Engineer.

ABSTRACT

Metallurgical examinations and evaluations were performed on a group of four target tubes from Atomic Power Development Associates (APDA) Rig 10. This group included two 2-1/4 Cr - 1 Mo ferritic steel tubes, one Type 304 SS, and one Incoloy 800 tube. These tubes had been exposed to small leaks of water in 600°F sodium.

Metallographic data indicate that the material loss (wastage) was primarily due to impact (or erosion) of liquid particles. No evidence of corrosion was found in the wasted areas of any target tubes. Minor corrosion was observed on the outside diameter of the austenitic stainless-steel tubes only in areas away from impact; no corrosion was detected on the outside diameter of the ferritic steel tubes.

Hardness measurements and microstructural analyses revealed that the maximum temperature may have reached 1600°F in the wasted areas. This localized temperature increase appeared to enhance the wastage process for all target tubes regardless of composition. Surface grain elongation and plastic deformation lines were observed in wasted areas, as well as in other areas. However, their cause(s) cannot be ascertained with respect to deformation due to water-jet impact, or deformation due to fabrication and handling, or both.

Based on the volumetric measurements of the wastage zones produced, Incoloy 800 (tube No. 21) exhibited greater resistance to water-jet impact/erosion (penetration depth ~0.011 in. in 570 sec), while 2-1/4 Cr - 1 Mo ferritic steel displayed the least (depth of penetration 0.064 in. in 21 sec).

I. INTRODUCTION

Four target tubes (tested under the APDA Small Leak Sodium-Water Reaction Program) were received from APDA for metallurgical examination. The target tubes included two 2-1/4 Cr - 1 Mo ferritic steel tubes (1-in. OD x 1/8-in. wall x 7 in. long), one Type 304 SS tube (1 in. OD x 1/8-in. wall x 7 in. long), and one Incoloy 800 tube (7/8 x 1/8 x 4 in.). Their compositions are shown in Table 1. The target tubes were exposed to water-jet impact and sodium-water reactions in APDA's Rig 10. The test conditions and results are summarized in Table 2.

The objective of this evaluation was to characterize the nature of wastage damage of the four tubes. The scope of work included:

1) Measurement of the extent of corrosion and/or erosion.

2) Determination of the nature of corrosion.

3) Assessment of the contribution of erosion to the total wastage process.

4) Determination of the contribution of plastic straining due to water-jet impact and subsequent thermal surge resulting from sodium-water reactions.

5) Determination of the maximum temperature reached by the affected material in the target area.

TABLE 1

COMPOSITIONS OF THE EXPOSED TARGET TUBE MATERIALS*

Element (wt %)	Tube No. 15 (2-1/4 Cr - 1 Mo)	21 (Incoloy 800)	29A (Type 304 SS)	37 (2-1/4 Cr - 1 Mo)
Cr	2.26	19.03	19.2	2.10
Ni	0.12	32.99	9.3	0.10
C	0.11	0.08	0.07	0.11
Mo	1.01	-	-	1.02
Mn	0.54	0.85	1.85	0.56
Si	0.28	0.56	0.50	0.36
Fe	Balance	Balance	Balance	Balance
Al	-	0.39	-	-
Ti	-	0.53	-	-
S	0.015	0.014	-	0.020
P	0.019	0.010	-	0.026

*Chemical analyses were performed on sections away from impact.

TABLE 2

DATA SUMMARY FOR APDA SAMPLES(1)

Test Results and Conditions	Tube No. 15 (2-1/4 Cr - 1 Mo)	Tube No. 21 (Incoloy 800)	Tube No. 29A (Type 304 SS)	Tube No. 37 (2-1/4 Cr - 1 Mo)
RESULTS				
Wastage				
Area (in.^{2})	0.638	0.103	0.769	1.079
Volume in.^{3} (cc)	0.61×10^{-3} (0.010 cc)	0.36×10^{-3} (0.006 cc)	1.62×10^{-3} ($\sim$0.027 cc)	2.61×10^{-3} (0.043 cc)
Position (relative to target point)	On	Glancing	Glancing	Glancing
Morphology of damaged area	Shallow Pit	Broad Pit	Shallow Pit, Little Erosion	Off-Center Pit
CONDITIONS				
Sodium System				
Flowrate (gpm)	0	400	400	400
Velocity past target tube (ft/sec)	0	2	2.0	2.0
Bulk temperature (°F)	610	400	610	600
Sodium level above target tube (ft)	8.4	-	-	-
Injection Water System				
Water added (lb)	0.24	1.3	1.3	0.197
Temperature (°F)	610	600	610	600
Pressure (psig)	2650	2650	2650	2650
Orifice size (in.)	0.006	0.006	0.016	0.010
Injection point to target spacing (in.)	1/4	1/4	1/4	1/4
Injection duration (sec)	125	570	150.5	20.9
Injection rate (lb/sec)	0.0019	0.0022	0.0086	0.0094
Wastage (APDA Data)				
Depth of penetration (mil)	12	12	21	63
Wastage rate (mil/sec)	0.10	0.02	0.140	3.0
Wastage rate (mil/lb-H_2O)	50	9.2	16.2	320
Maximum measured tube temperature (°F)	1380	1341	1600	1580

Notes: Type 304 SS and 2-1/4 Cr - 1 Mo target tubes were 1.0-in. OD x 0.120-in. wall. Incoloy 800 was 0.84-in. OD x 0.109-in. wall.

II. EXPERIMENTAL

A. DIMENSIONAL AND VOLUMETRIC MEASUREMENTS

The extent of erosion/corrosion was determined by dimensional and volumetric measurements. Dimensional measurements (maximum length, width, and depth of the impacted area) were made from Coecal castings of the impacted areas by using a Scherr microprojector (precision ~ ±0.001 in.). Volume of the affected areas was measured from Cerrobend impressions of the indented areas. Cerrobend (a bismuth-base alloy) was used because of its low melting point (~158 °F). Castings were made at 160 °F and were shaped (filed) at room temperature to match the contour of the tubes; a Scherr microprojector was used to assure dimensional accuracy. After the castings were made, the volume of wastage was measured at room temperature by immersing the Cerrobend impression in a graduated 10-cc burette (precision ~ ±0.010 cc) containing a known level of water. The net volume of the impacted area (or the Cerrobend casting) was determined by fluid displacement in the graduated burette.

B. HEAT TREATMENT

To determine the maximum temperature reached by the four target tubes, standards were made using sections of each exposed tube material remote from the impact area. These small tube sections (1/2 x 1/2 x 1/8 in.) were quenched from various elevated temperatures (1200 to 2100 °F at 100 °F intervals) to 600 °F in a helium atmosphere. The test matrix for this series of heat-treating experiments is shown in Table 3.

The heat treatment was conducted in a Type 304 SS retort with the capability of quenching four samples (coupons) simultaneously. Figure 1 shows the cylindrical retort (~1-in. ID x 1/16 in. wall x 48 in. long), the sample holder, the four thermocouple wells, and the Conoseal used to maintain inert atmosphere in the retort. The test setup, with retort installed in the two 3-zone furnaces, is shown in Figure 2. Accurate temperatures (±5 °F) in the two isothermal zones were monitored by three calibrated thermocouples: one Chromel-Alumel thermocouple in the low isothermal zone (600 °F), and two platinum-platinum/10% Rh thermocouples (with one in the high-temperature zone, and the other attached to the sample holder next to the specimens).

TABLE 3

TEST MATRIX

Batch No.	Tempering Temperature (°F)	Time at High Temperature (min)	Tube Sample Number			
			15	21	29A	37
1	1800	5	55.5A*	15.5A*	95.5A*	77.5A*
1A	1800	2	56A	-	-	-
1B	1800	10	55.5H	15.5H	95.5A	77.5H
2	1700	5	55.5B	15.5B	95.5B	77.5B
2A	1700	2	56B	-	-	-
2B	1700	10	56C	-	-	-
3	1600	5	55.5C	15.5C	95.5C	77.5C
3A	1600	2	56D	-	-	-
3B	1600	10	-	-	-	-
4	1500	5	55.5D	15.5D	95.5D	77.5D
4A	1500	2	-	-	-	78B
4B	1500	10	-	-	-	-
5	1400	5	55.5E	15.5E	95.5E	77.5E
5A	1400	2	-	-	-	78C
5B	1400	10	-	-	-	78E
6	1300	5	55.5F	15.5F	95.5F	77.5F
6A	1300	2	-	-	-	78F
6B	1300	10	-	-	-	78G
7	1200	5	55.5G	15.5G	95.5G	77.5G
7A	1200	2	-	-	-	78H
7B	1200	10	-	-	-	78A
8	1900	5	55A	15A	95.5A	75.5A
8A	1900	2	55B	15B	95.5B	75.5B
8B	1900	10	55C	15C	95.5C	75.5C
9	2000	5	55D	15D	95.5D	75.5D
9A	2000	2	55E	15E	95.5E	75.5E
9B	2000	10	55F	15F	95.5F	75.5F
10	2100	5	55G	15G	95.5G	75.5G
10A	2100	2	55H	15H	95.5H	75.5H
10B	2100	1	-	-	-	76B

*Numerical values represent sample location.

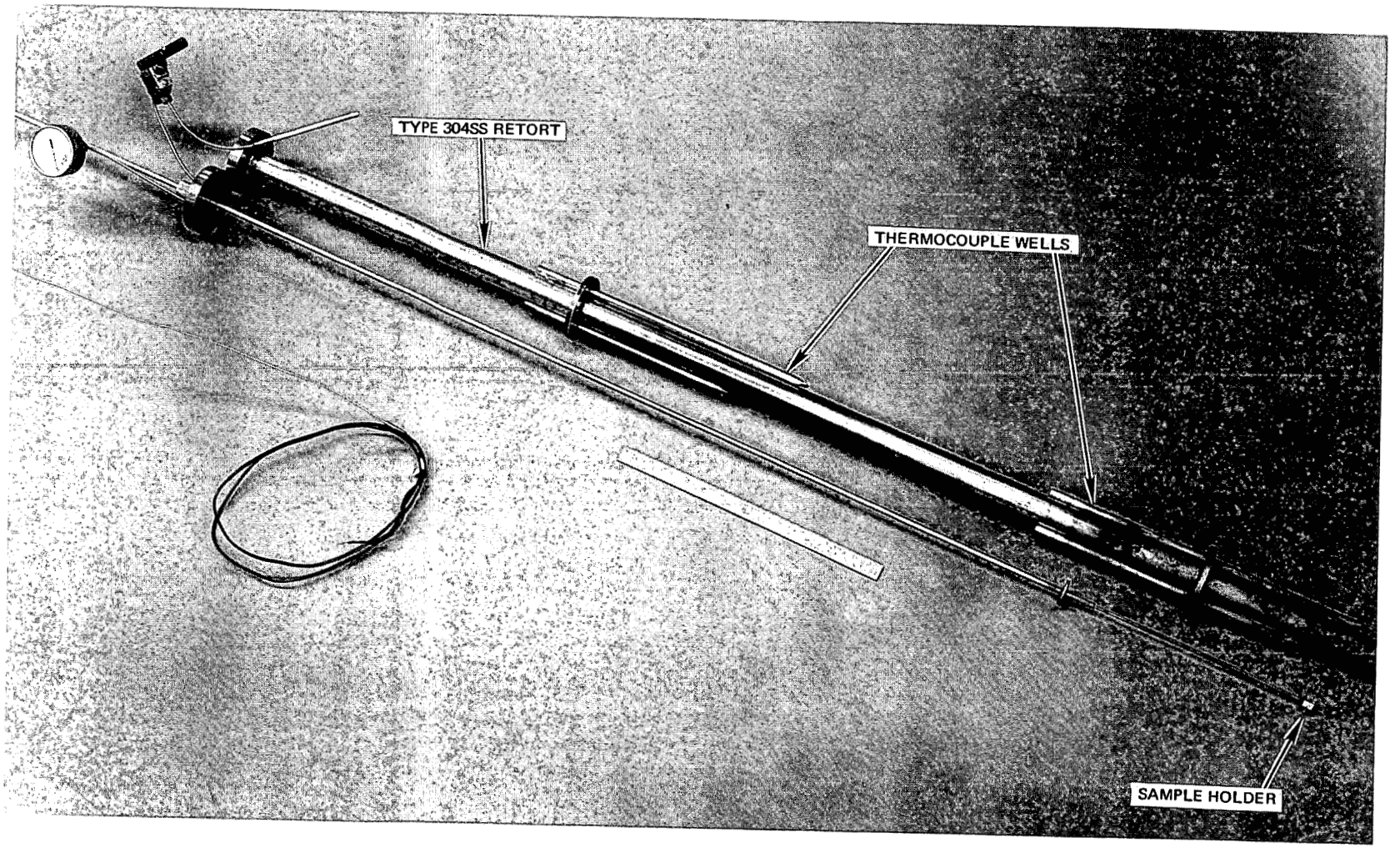

Figure 1. Retort and Sample Holder for the Quenching Experiment

7694-40347

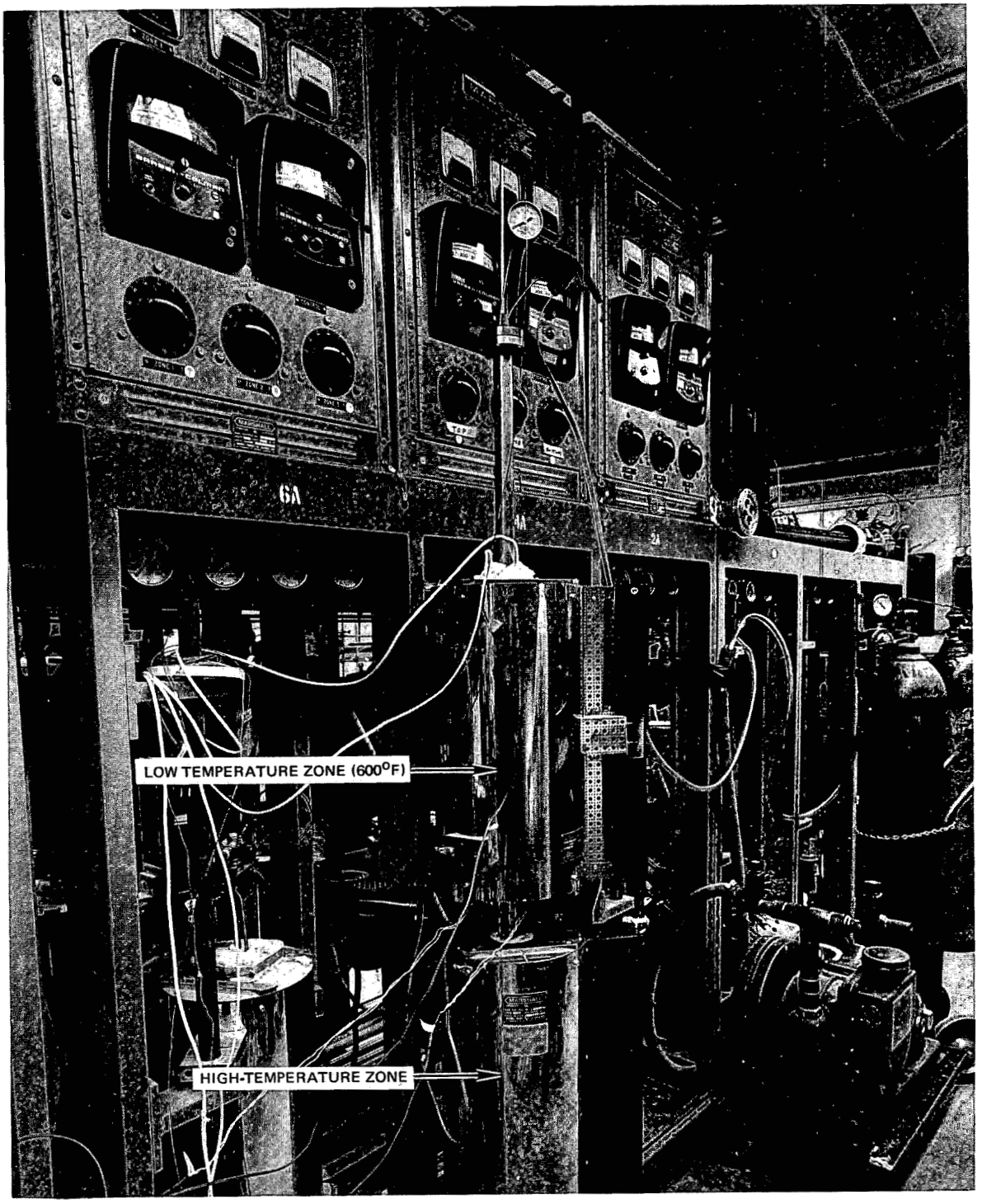

7694-40345

Figure 2. Quenching Apparatus with Retort Installed in Furnaces

Subsequent to sample loading in the low-temperature zone and prior to insertion of the sample in the high-temperature zone, the retort system was evacuated and purged clean with high purity helium. A helium pressure of about 10 psig was maintained during the quenching process. After the samples reached thermal equilibrium at 600°F (~20 min), the sample rod with four samples was quickly lowered to the high-temperature zone for soak durations of 2, 5, or 10 min, as shown in Table 3. After the prescribed soaking time, the sample rod was again quickly retrieved to the low-temperature zone (600°F) for quenching. The samples were again left in the low-temperature zone for approximately 40 min, until the sample temperature equilibrated to ~600°F. The total transient time involved in raising or lowering the samples was about 1 sec, while the time required to reach thermal equilibrium at the prescribed high-temperature zone was about 8 min. A typical heating and cooling cycle for a quench is shown in Figure 3.

C. METALLOGRAPHIC SAMPLE PREPARATION

Due to the small size of the indented areas, the metallographic samples were sectioned by a special 10-mil-thick milling cutter. After being sectioned, the samples were mounted for metallography and hardness measurements. Nital was used for etching 2-1/4 Cr - 1 Mo ferritic steel and Marble's Reagent for both austenitic steels.

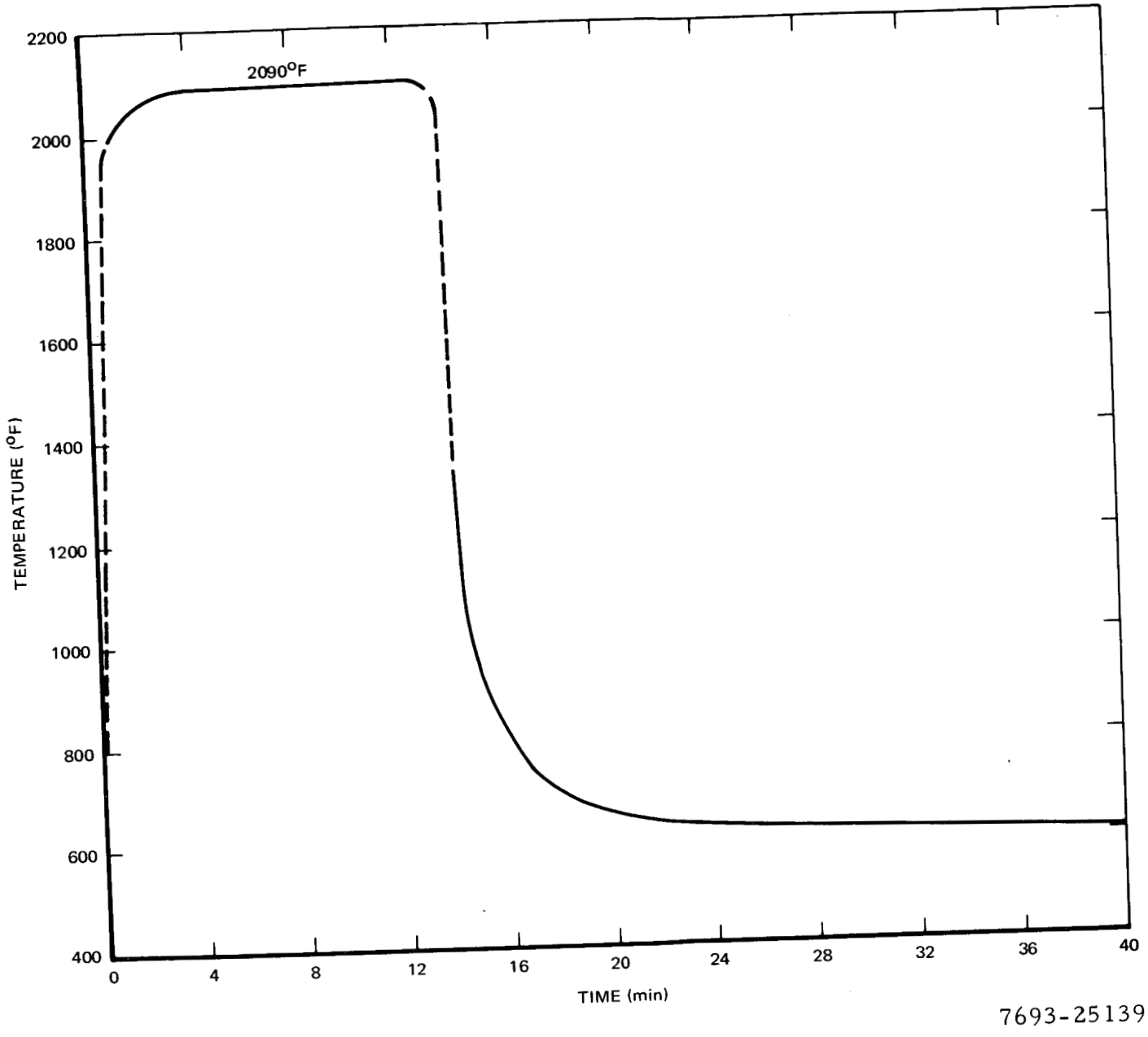

Figure 3. Typical Thermal History for a Batch of Four Specimens (Batch No. 10, 5-min Soak)

III. RESULTS

A. EXTENT OF MATERIAL WASTAGE

The extent of material wastage due to erosion/corrosion was determined by dimensional and volumetric measurements. The results of these measurements are shown in Tables 4 and 5. Of the three materials tested, 2-1/4 Cr - 1 Mo steel was the least resistant material and Incoloy 800 was the most resistant.

B. METALLOGRAPHY OF CONTROL (QUENCHED) SAMPLES

As shown in Table 3, a total of 76 samples were quenched from various high temperatures (1200 to 2100°F) to 600°F, involving 30 quenches in a helium environment. Forty-four of the 76 samples were 2-1/4 Cr - 1 Mo steel, 16 were Type 304 SS, and 16 were Incoloy 800. Detailed descriptions of the metallographic results for each material are presented in the following.

1. 2-1/4 Cr - 1 Mo Ferritic Steel

Metallographic examination of the quenched samples revealed the following:

1) Microstructure of the samples quenched from temperatures above 1800°F (i.e., 1900, 2000, and 2100°F) consisted primarily of tempered, fine, acicular bainite; probably a combination of martensite and fine bainite, as shown in Figure 4.

2) Microstructure of samples quenched from 1700 and 1800°F was composed principally of coarse and tempered bainite, a microstructure of iron carbide and ferrite (Figure 5). The carbide precipitation was located in both grain boundaries and grain matrix.

3) Photomicrographs of specimens quenched from 1600°F, or lower temperatures, displayed a microstructure of bainite and large proeutectoid ferrite grains, as shown in Figure 6. Some undissolved carbides were observed in specimens quenched from lower temperatures (below 1400°F).

TABLE 4

DIMENSIONS OF IMPACTED AREAS FOR FOUR RIG 10 TARGET TUBES

Dimension*	Tube No. 15 (2-1/4 Cr - 1 Mo Steel)	21 (Incoloy 800)	29A (Type 304 SS)	37 (2-1/4 Cr - 1 Mo Steel)
Maximum Depth (in.)	0.012	0.011	0.021	0.064†
Maximum Length (in.)	0.070	0.080	0.340	0.260
Maximum Width (in.)	0.082	0.125	0.095	0.072

*Minimum readable scale division 0.001 in.
†The maximum depth was confirmed by metallography.

TABLE 5

VOLUME OF IMPACTED AREAS FOR FOUR RIG 10 TARGET TUBES

10-cc Burette*	Tube No. 15 (2-1/4 Cr - 1 Mo Steel)	21 (Incoloy 800)	29A (Type 304 SS)	37 (2-1/4 Cr - 1 Mo Steel)
Original Volume of Water (cc)	-	-	4.00	3.975
Final Volume of Water (cc)	-	-	3.975	3.915
Volume of Affected Area (cc)	0.002†	0.005†	0.025	0.060

*Measured in 10-cc burette (minimum readable scale division = 0.01-cc). Impression was made of Cerrobend at ~ 160 °F, and then was filed to the contour of the tubing. The contour was checked with a Scherr microprojector.
†Calculated values based on dimensional measurement.

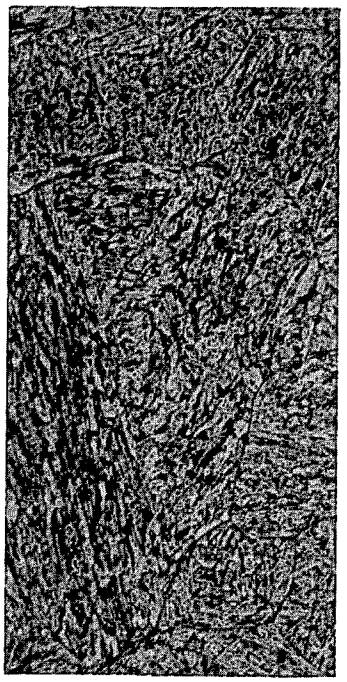

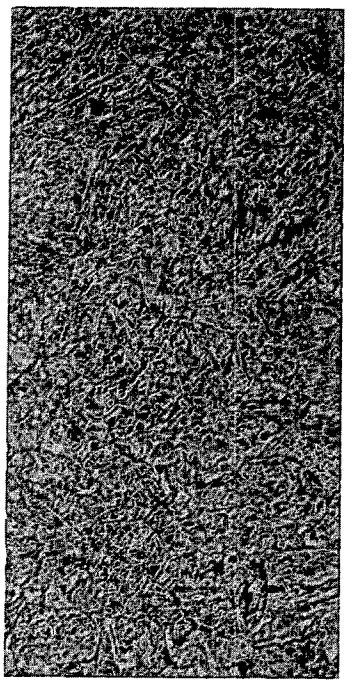

500X 7693-25140

a. 2000 °F (2-min Soak) b. 1900 °F (2-min Soak)

Figure 4. Microstructures of 2-1/4 Cr - 1 Mo Steel Quenched to 600 °F

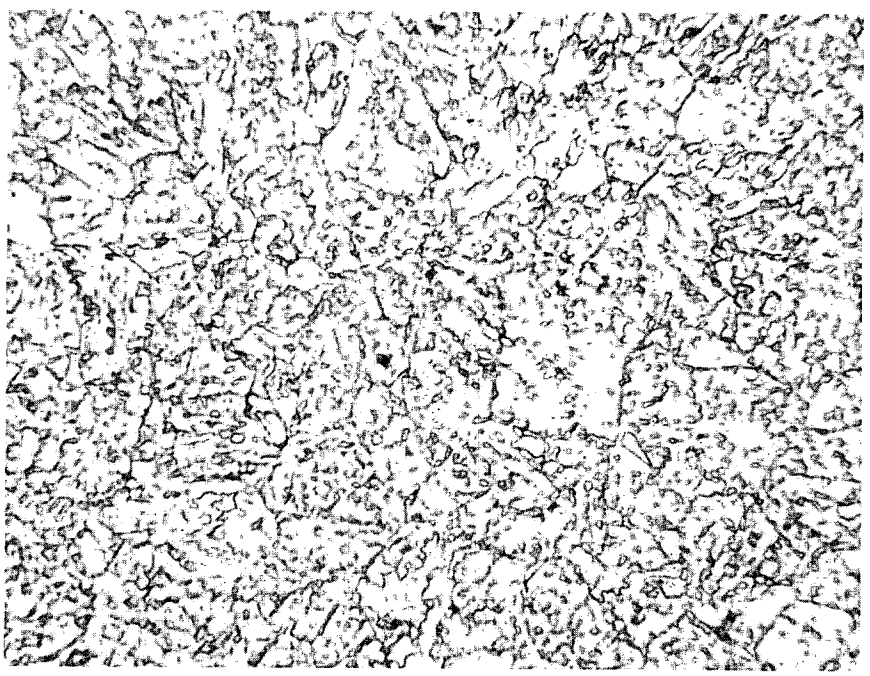

1000X 7693-25141

Figure 5. Microstructure of 2-1/4 Cr - 1 Mo Steel Quenched from 1800 °F to 600 °F in a Helium Environment

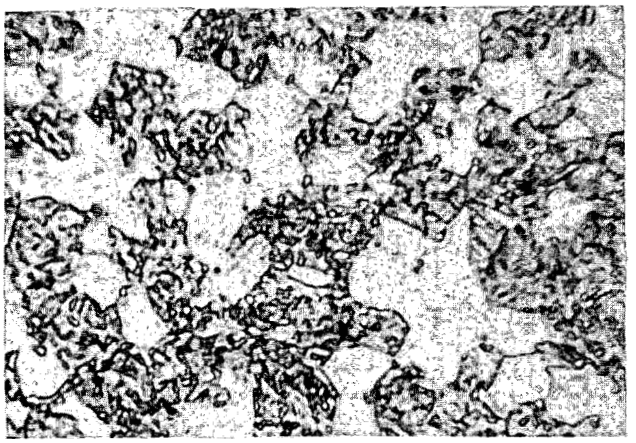

a. 1600 °F

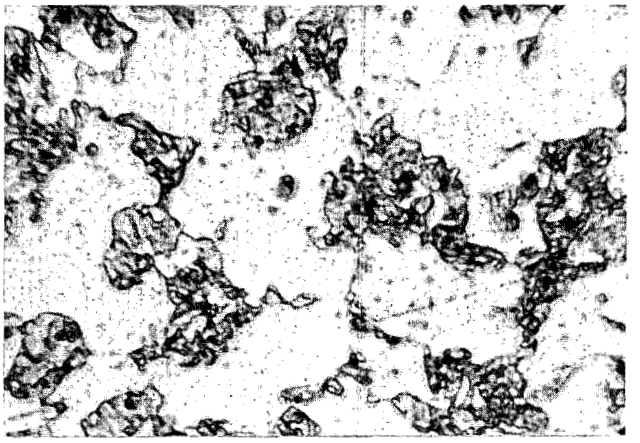

b. 1500 °F

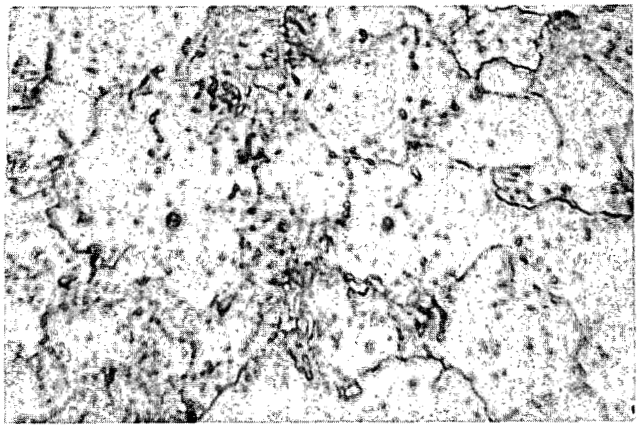

c. 1400 °F

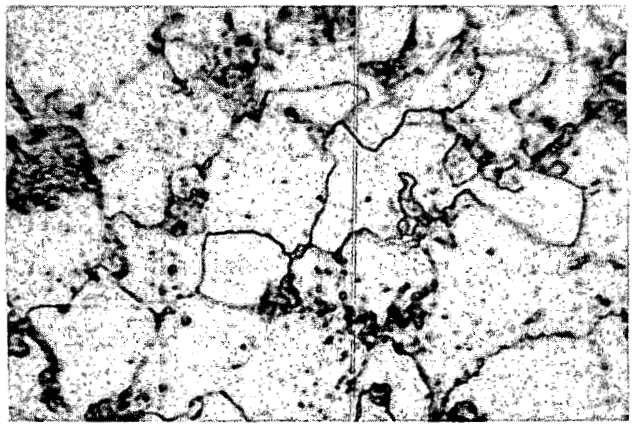

d. 1300 °F

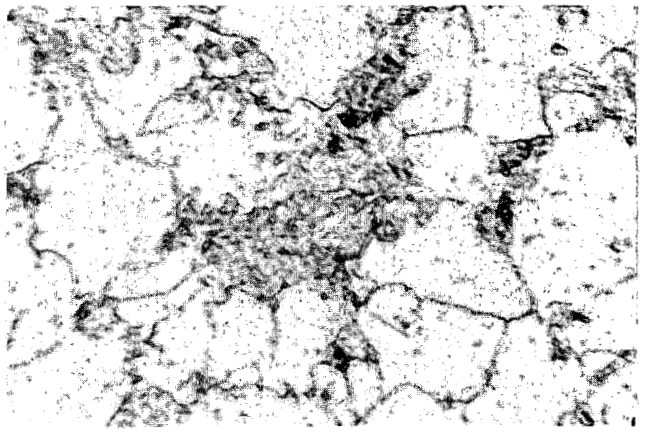

1000X

7693-25142

e. 1200 °F

Figure 6. Microstructure of 2-1/4 Cr - 1 Mo Steel Quenched from Various High Temperatures to 600 °F in a Helium Environment (5-min Soak)

4) In addition to carbides and ferrites, second-phase particles, possibly retained austenite, were observed in all the quenched samples. Specifically, in samples quenched from below 1700°F, the distribution of second-phase particles appears to be localized in the bainite areas and not in proeutectoid ferrite grains (Figure 6). In samples quenched at or above 1700°F, the distribution of second-phase particles was not localized but was found randomly in grain matrix and grain boundaries, as shown in Figure 5.

5) The effect of quenching temperature on the average room temperature hardness of 2-1/4 Cr - 1 Mo steel is shown in Figure 7.

2. Incoloy 800

Microstructure of Incoloy 800 control samples quenched from various high temperatures to 600°F displayed the following:

1) A discontinuous carbide network in grain boundaries and in slip lines on samples quenched from 1200°F to 1600°F (Figure 8). Some localized grain elongation and plastic deformation lines were also observed on the outside diameter of tubes. For samples quenched from 1700°F, some grain boundary carbides began to disappear, resulting in a diffuse grain boundary. Grain growth and depletion of grain boundary carbides are apparent in samples quenched from 1800°F and higher temperatures (Figure 8h and i). No grain boundary carbides were observed on samples quenched above 1800°F.

2) The effect of quenching temperature on room temperature hardness values of Incoloy 800 is shown in Figure 9. As expected, the room temperature hardness is insensitive to quenching temperature. It is interesting to note, however, that the room temperature hardness began to decrease above 1800°F, which is consistent with the observations of grain growth and the dissolution of grain boundary carbides around 1800°F.

3. Type 304 SS

Metallographic examination of Type 304 SS samples quenched from various high temperatures (1200 to 2100°F for 5 min) to 600°F revealed the following (Figure 10):

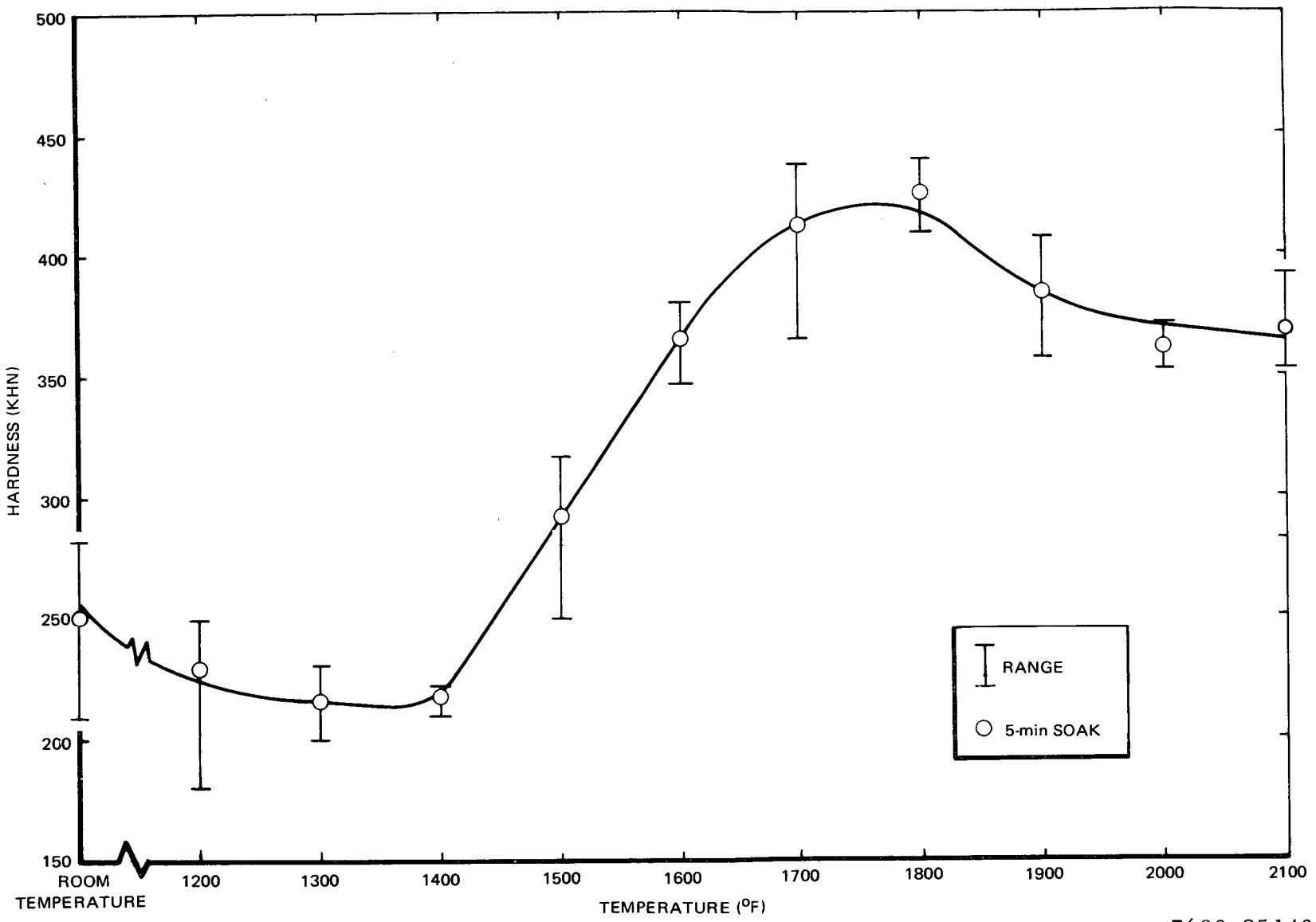

7693-25143

Figure 7. Effect of Quench Temperature on Average Room Temperature Hardness of 2-1/4 Cr - 1 Mo Steel

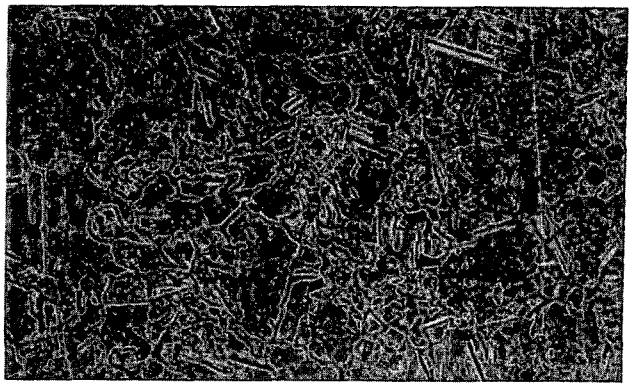

a. 1200 °F

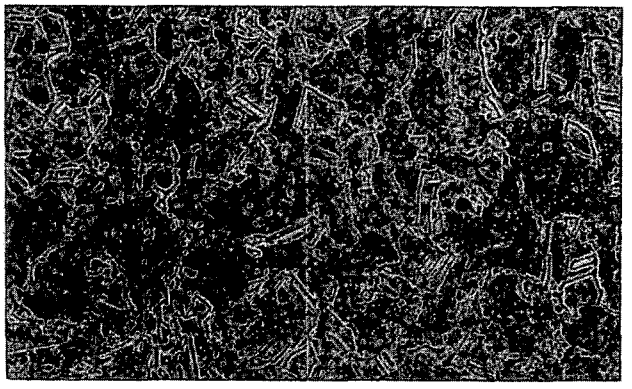

b. 1300 °F

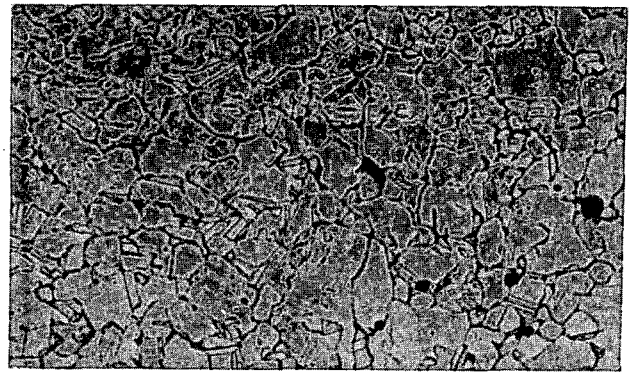

c. 1400 °F

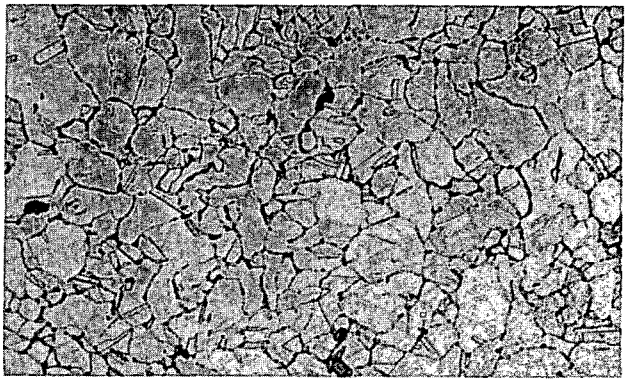

d. 1500 °F

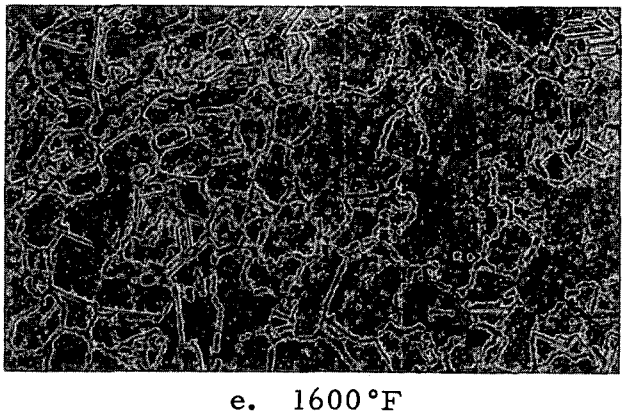

e. 1600 °F

500X

7693-25144-1

Figure 8. Microstructure of Incoloy 800 Quenched from Various High Temperatures to 600 °F in Helium (5-min Soak) (Sheet 1 of 2)

f. 1700°F

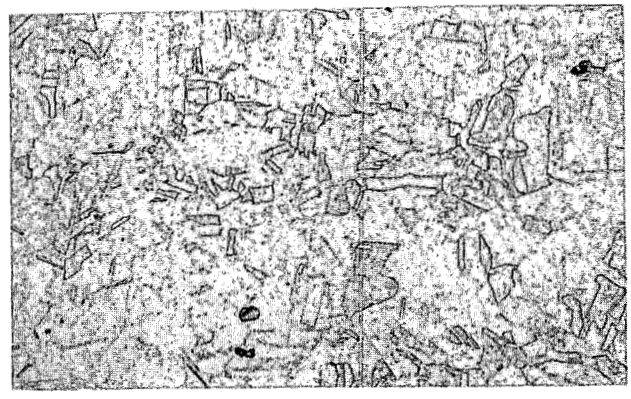

g. 1800°F

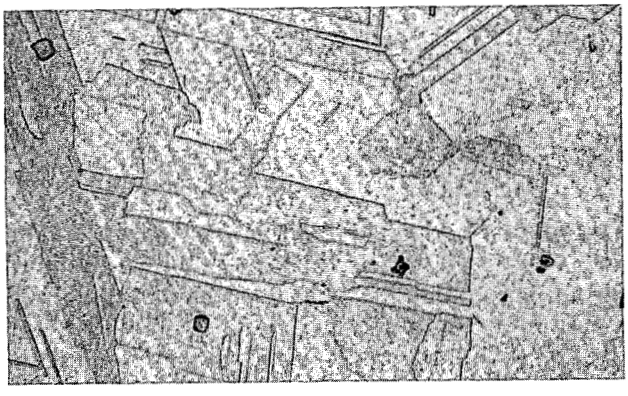

h. 1900°F

i. 2000°F

500X

7693-25144-2

Figure 8. Microstructure of Incoloy 800 Quenched from Various High Temperatures to 600°F in Helium (5-min Soak) (Sheet 2 of 2)

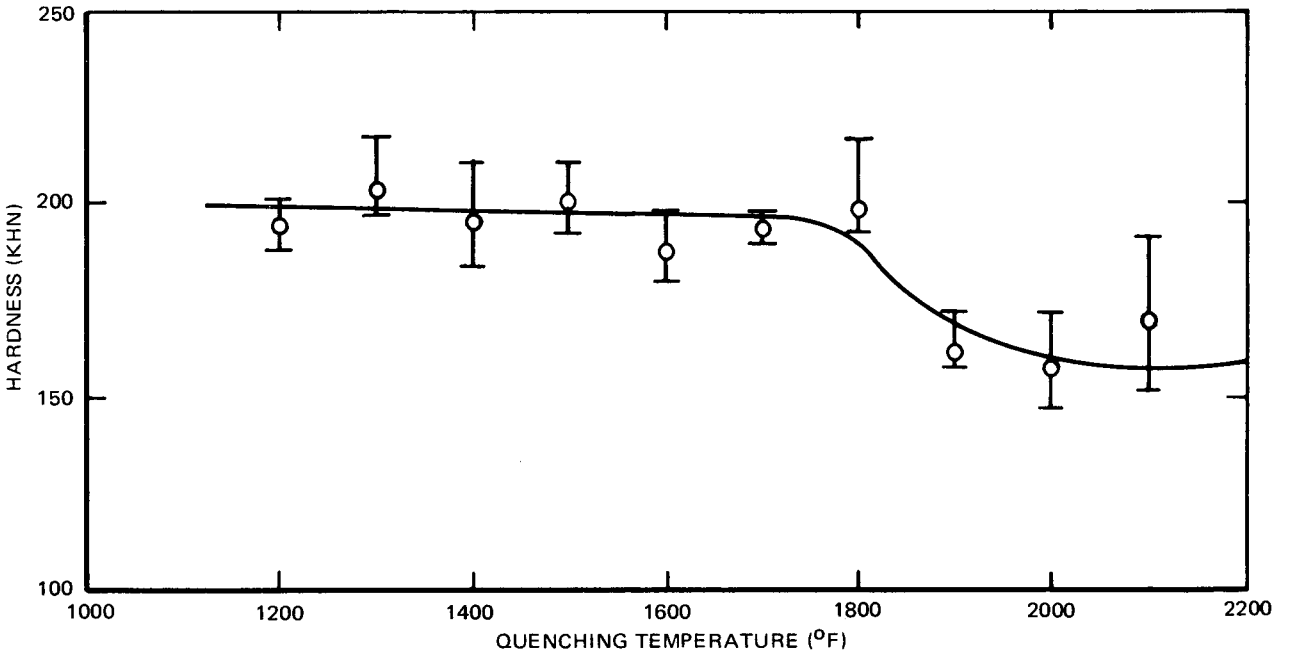

7693-25145

Figure 9. Effect of Quenching Temperature on Room Temperature Hardness of Incoloy 800

1) For a 5-min soak at 1200°F, the Type 304 SS sample exhibited little or no observable carbide precipitation along grain boundaries or in the grain matrix.

2) For an equivalent soak time (i.e., 5 min) at higher temperatures (from 1300 to 1700°F), dense carbides were observed along grain boundaries, twin boundaries, and deformation bands. At 1700 and 1800°F, with an equivalent soak time, carbides started to redissolve resulting in a decreased carbide density. At 1900°F, grain growth commenced with complete dissolution of grain boundary carbides.

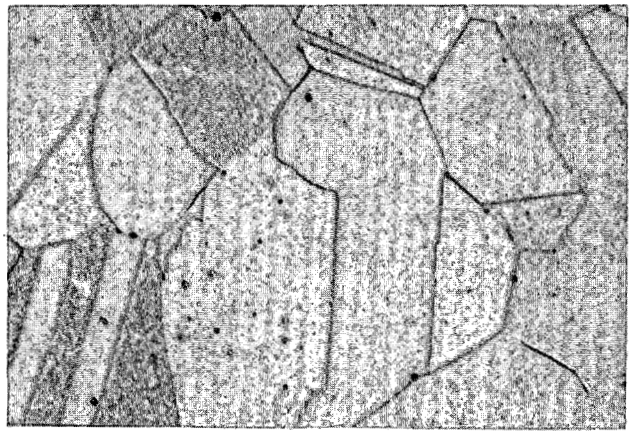

a. 1200°F 500X

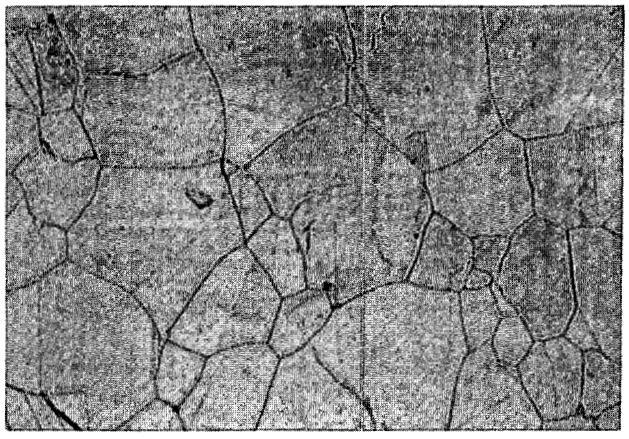

b. 1300°F 250X

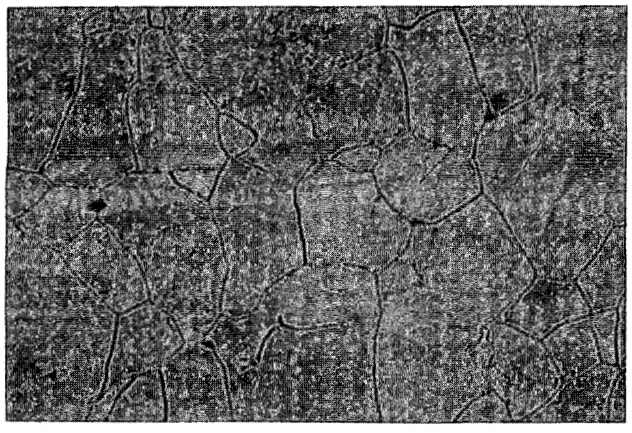

c. 1400°F 250X

d. 1500°F 250X

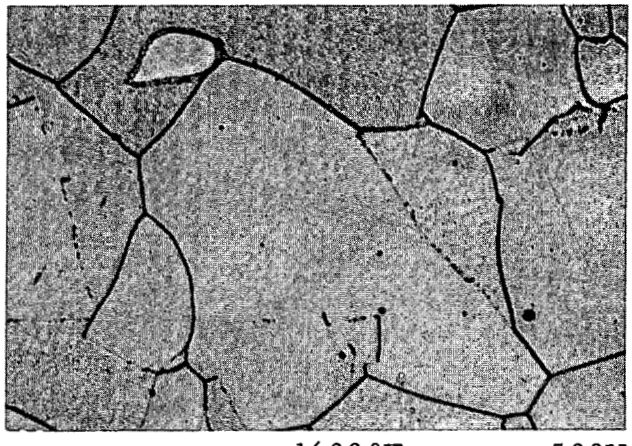

e. 1600°F 500X

7693-25146-1

Figure 10. Microstructure of Type 304 SS Quenched from Various High Temperatures to 600°F in Helium (5-min Soak)
(Sheet 1 of 2)

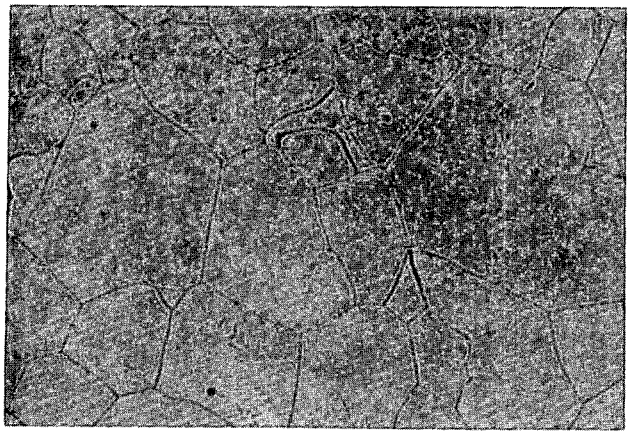

f. 1700°F 250X

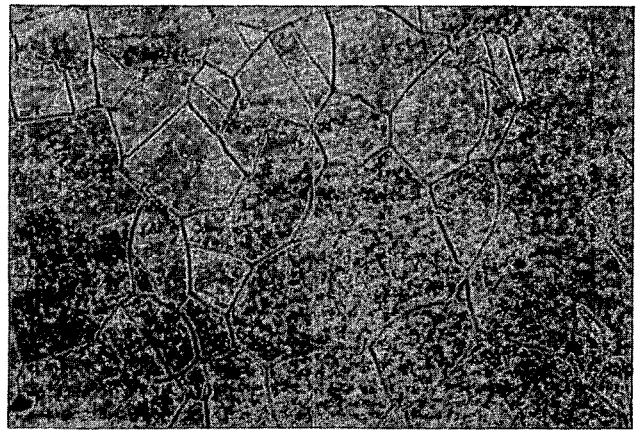

g. 1800°F 250X

h. 1900°F 250X

i. 2000°F 250X

7693-25146-2

Figure 10. Microstructure of Type 304 SS Quenched from Various High Temperatures to 600°F in Helium (5-min Soak)
(Sheet 2 of 2)

C. EXAMINATION OF AFFECTED AREAS IN THE TARGET TUBES

1. Tube No. 37 (2-1/4 Cr - 1 Mo Ferritic Steel)

Figure 11 is a macrograph of the affected area (0.26 in. x 0.07 in. x 0.064 in.) on tube No. 37. The flow pattern, like a river delta, is particularly evident.

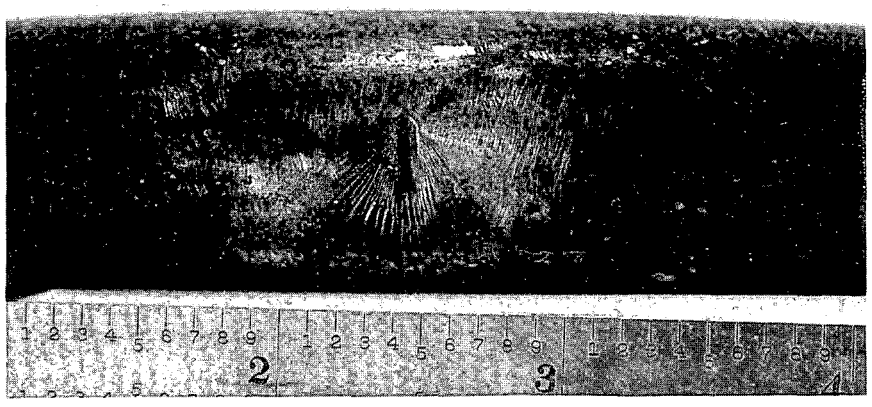

7693-25147

Figure 11. Ferritic Steel Tube Section Showing Area of Metal Removal (Wastage) After Steam Impingement in 600°F Sodium

Microstructural examination of tube No. 37 disclosed a general bainitic structure with large proeutectoid ferrite grains (Figure 12). In addition to the presence of undissolved carbides in the grains, an unknown second phase was observed in areas close to impact. When etched with Nital or Murakami, the second-phase particles were observed to be in relief, which indicates that the second-phase particles were not agglomerated carbide particles. It is believed that the second phase could be retained austenite.

Detailed microstructural examination of areas in and adjacent to the impact cavity did not reveal any corrosion products or corrosion/depletion layer. Moreover, no intergranular corrosion was observed on the outside diameter of the tube exposed to sodium-water reaction products. Although it was not observed on the impact areas, a decarburized layer (~ 3 mil thick) was observed on the outside diameter of the tube (Figure 13). This decarburized layer is not believed due to sodium-water reaction, but rather primarily a result of fabrication. Some deformation lines/bands and grain elongation were observed in the grains adjacent to the impacted areas (Figure 14).

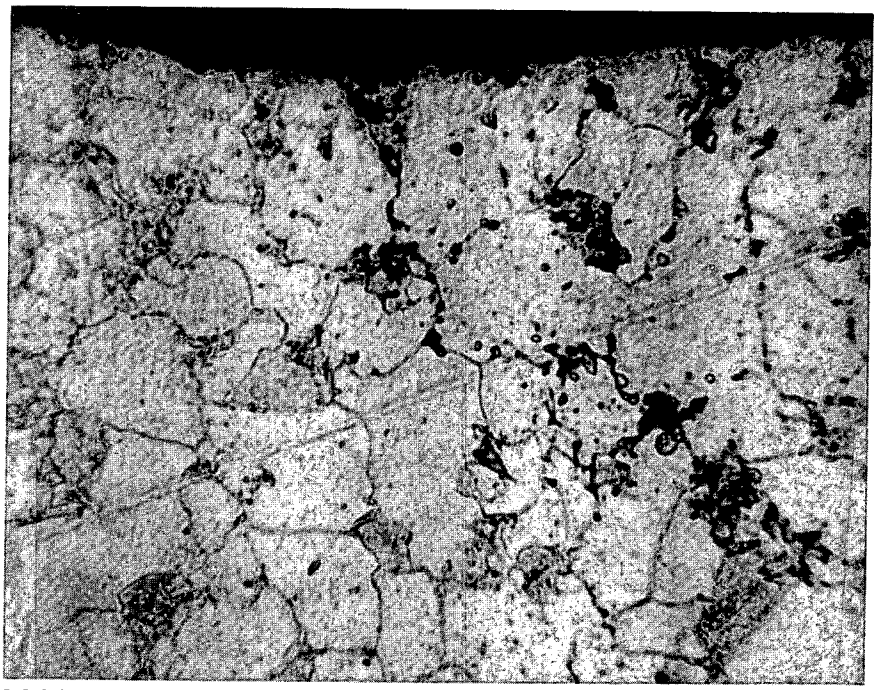

1000X 7693-25148

Figure 12. Microstructure of Impact Area of 2-1/4 Cr - 1 Mo Steel after Sodium-Water Reactions

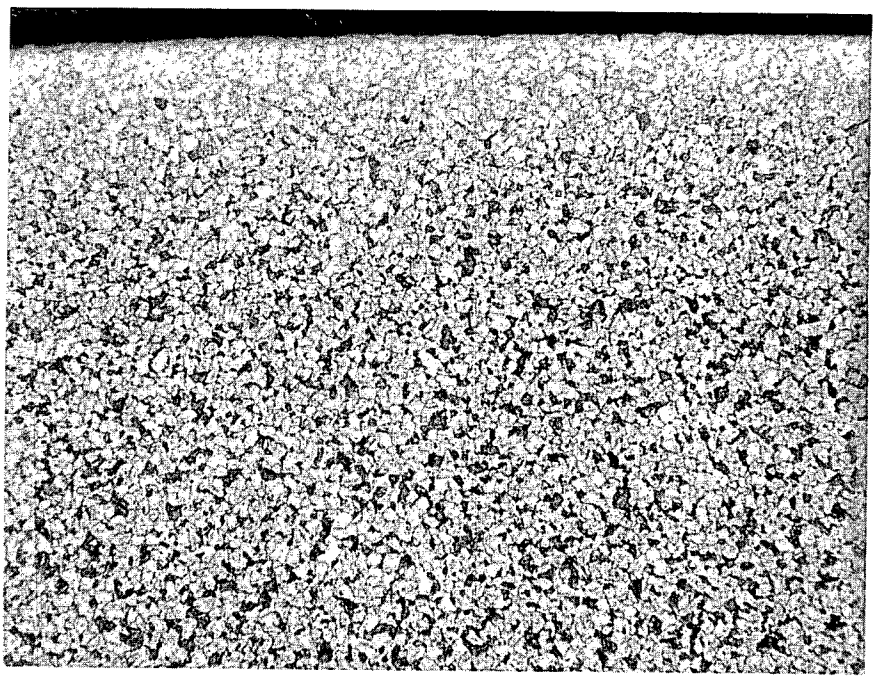

100X 7693-25149

Figure 13. Decarburized Layer (~3 mil thick) on Outside Diameter of Tube No. 37 in Areas Away from Impact Cavity

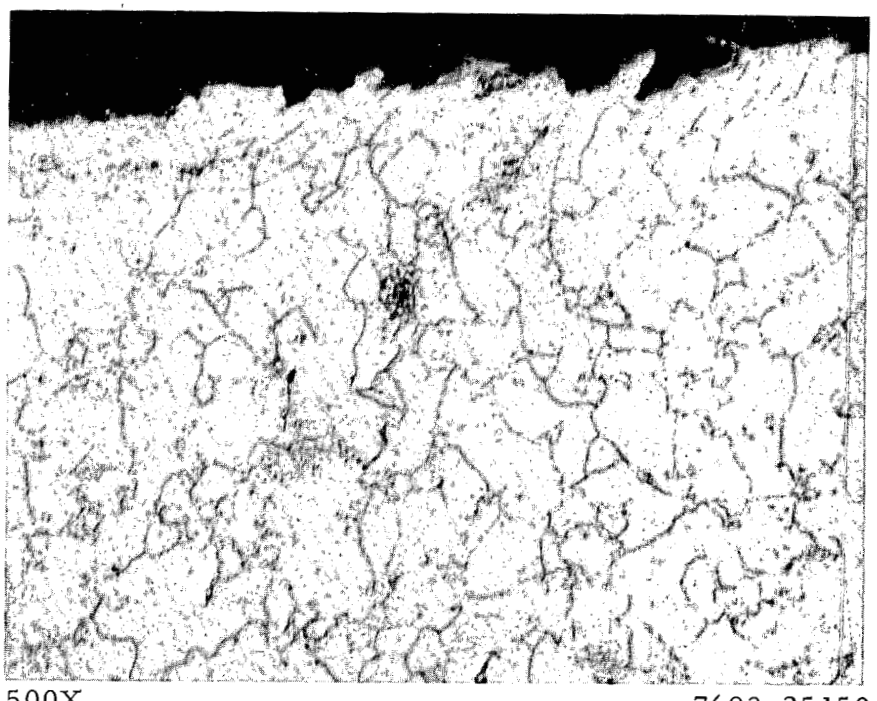

500X 7693-25150

Figure 14. Elongated Grains in Areas Adjacent to the Impact Area, Showing Plastic Deformation

From these observations, it can be concluded that erosion/impact was the controlling mechanism for the observed wastage. No corrosion was detected.

A detailed hardness measurement was performed on a specimen containing the impact cavity (Figure 15). In general, there are no significant variations in hardness between the impact areas and other areas away from impact. However, two locations beneath the impact areas showed a significant increase in hardness on the outside diameter (KHN 285 vs 253, and KHN 304 vs 253).

2. Tube No. 21 (Incoloy 800)

A macrograph of the impact area for tube No. 21 is shown in Figure 16. The size of impact indentation was 0.08 in. x 0.125 in. x 0.011 in. depth). The areas around the indentation had a polished and shiny appearance.

Microstructural examination of tube No. 21 disclosed:

1) Dense carbide precipitation on grain boundaries, and little precipitation on twin boundaries at the tube outside diameter (Figure 17),

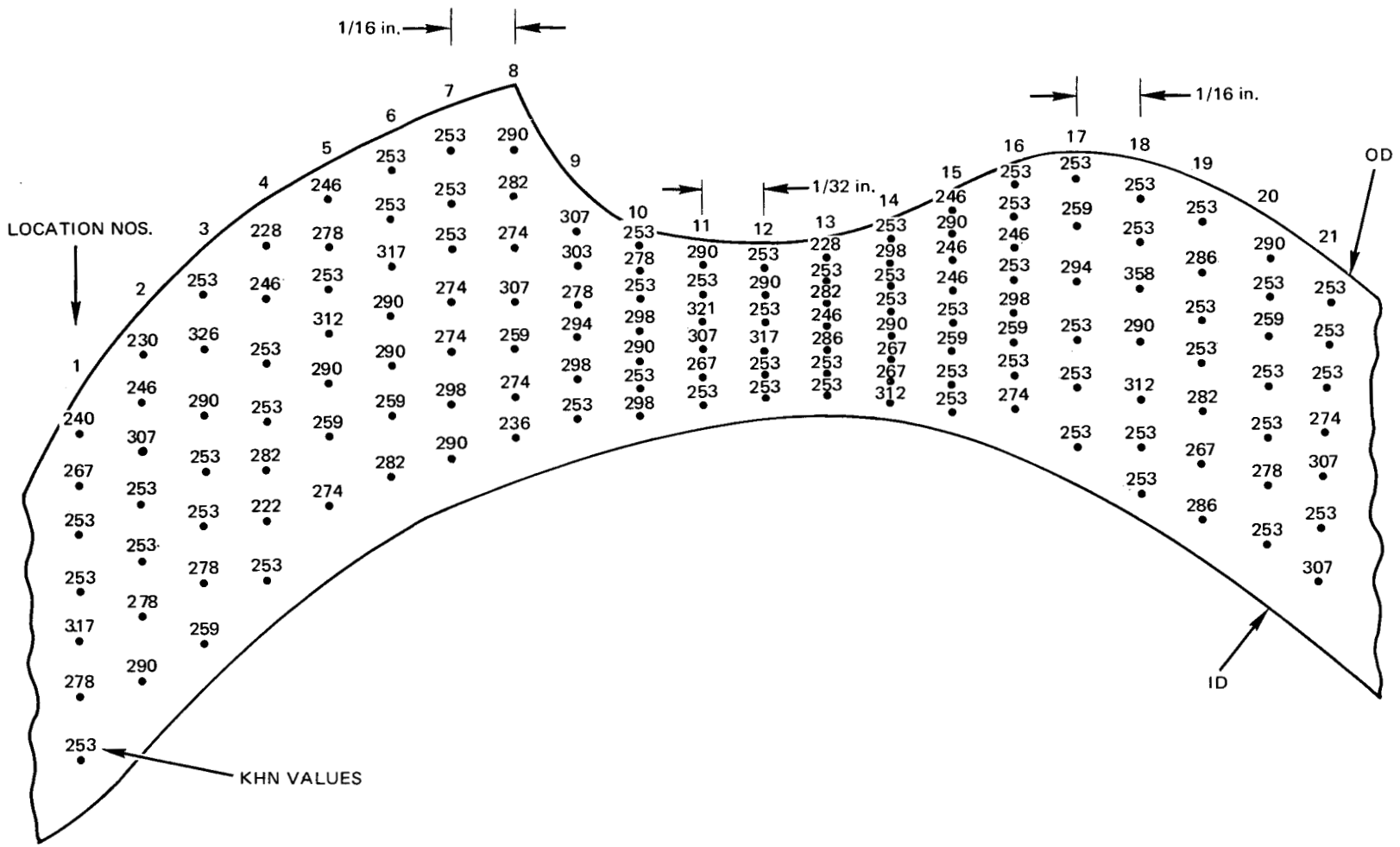

7693-25151

Figure 15. Knoop Hardness (KHN) Variation in Wasted Areas for Tube No. 37 (2-1/4 Cr - 1 Mo Ferritic Steel)

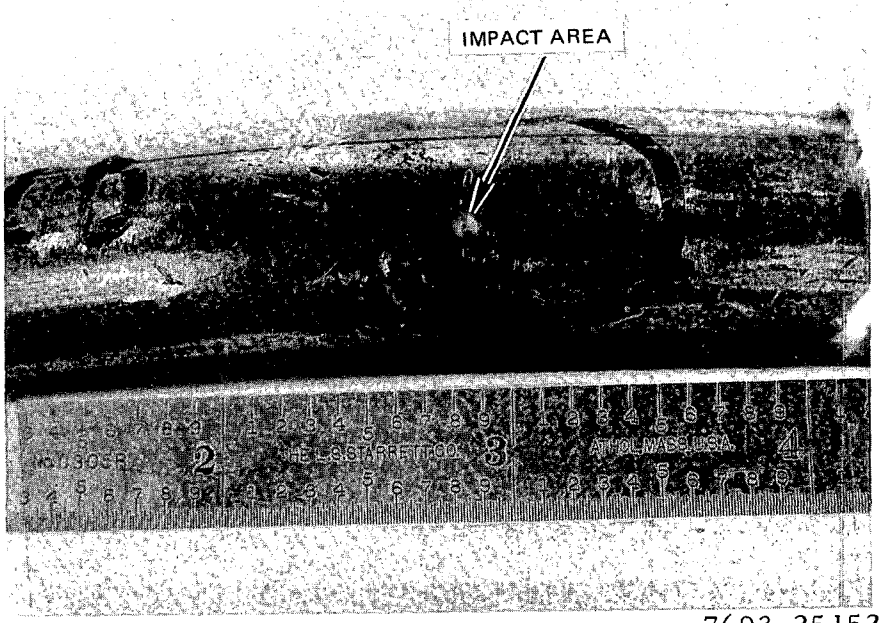

1.5X 7693-25152

Figure 16. Macrograph of Tube No. 21 (Incoloy 800) after Water-Jet Impact, Showing the Impact Indentation

a microstructure typical of sensitized Incoloy 800. This carbide precipitation occurred only within the outer one-third of the tube wall (i.e., ~1/24 in. thick). Areas adjacent to the inside diameter (covered about two-thirds of the tube wall) exhibited a cold-worked microstructure with longitudinal plastic flow lines resulting from fabrication. In these areas, carbide precipitation was relatively absent.

2) Areas close to the impact region exhibited deformation bands and elongated grains (Figures 18 and 19). These microstructural indications suggest apparent plastic straining and deformation, possibly due to impact loading. In addition to some minor intergranular corrosion (~ 1 grain thick) on the tube outside diameter away from impact (Figure 19), a discontinuous corrosion or depletion layer (~ 0.5 mil thick) was also observed (Figure 20). The depletion layer was found to be approximately 50% softer than the base material (Figure 21).

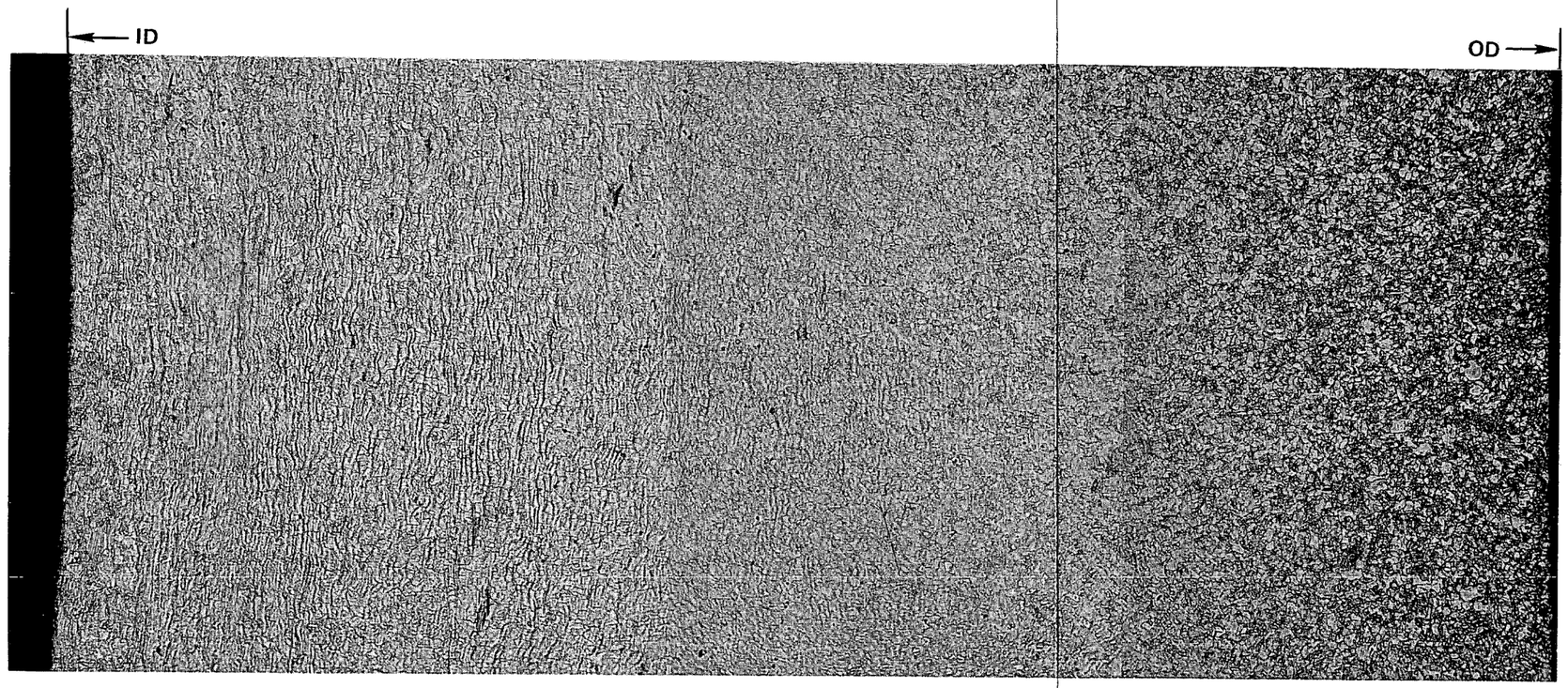

100X

7693-25153

Figure 17. Carbide Distribution in Incoloy 800 Exposed to Sodium-Water Reactions

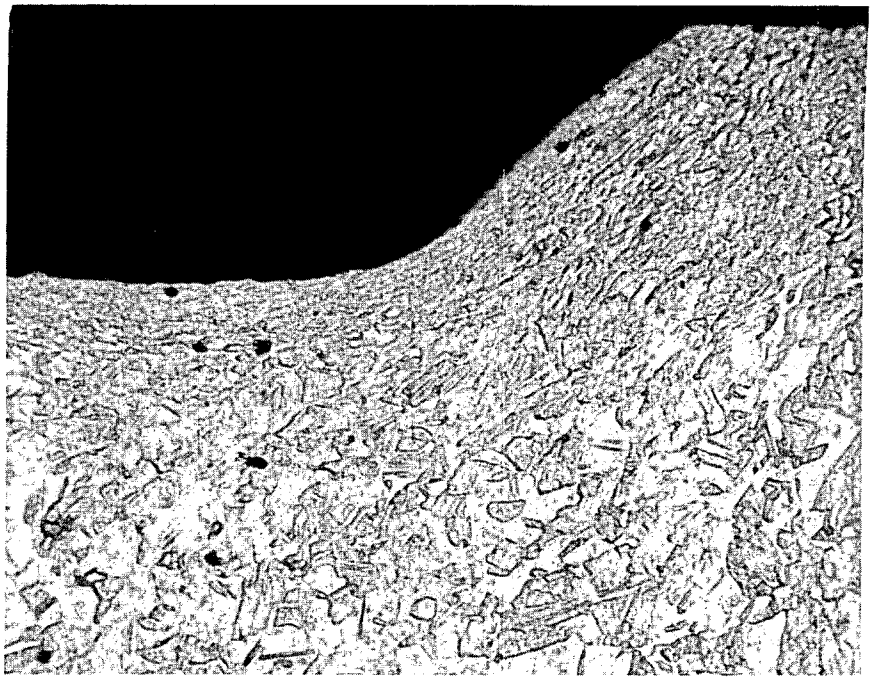

500X 7693-25154

Figure 18. Incoloy 800 Exposed to Sodium-Water Reactions, Showing the Elongated Grains in an Area Adjacent to the Impact

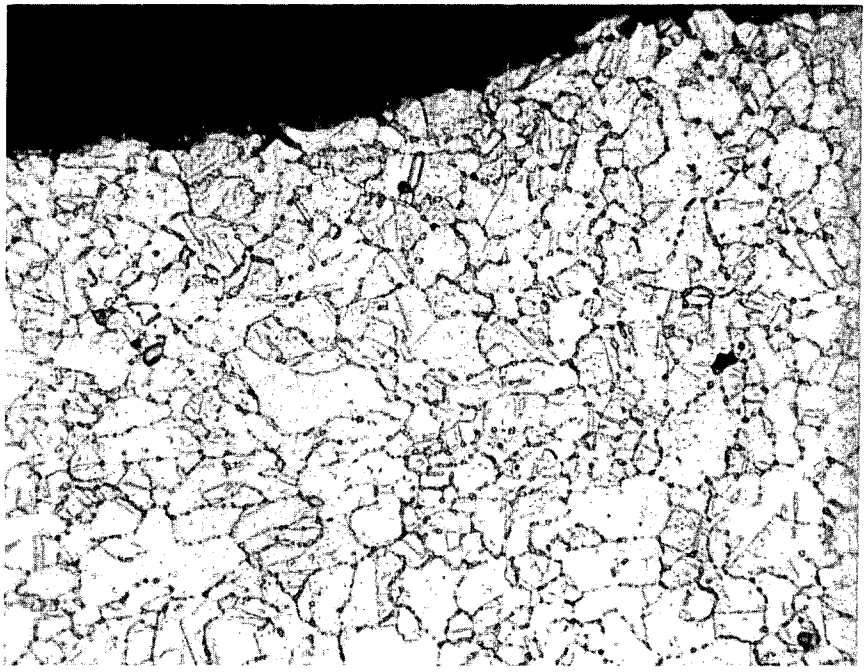

500X 7693-25155

Figure 19. Microstructure of Incoloy 800 Tube Exposed to Sodium-Water Reactions, Showing Carbide Precipitation and Minor Intergranular Corrosion on Tube Outside Diameter away from Impact

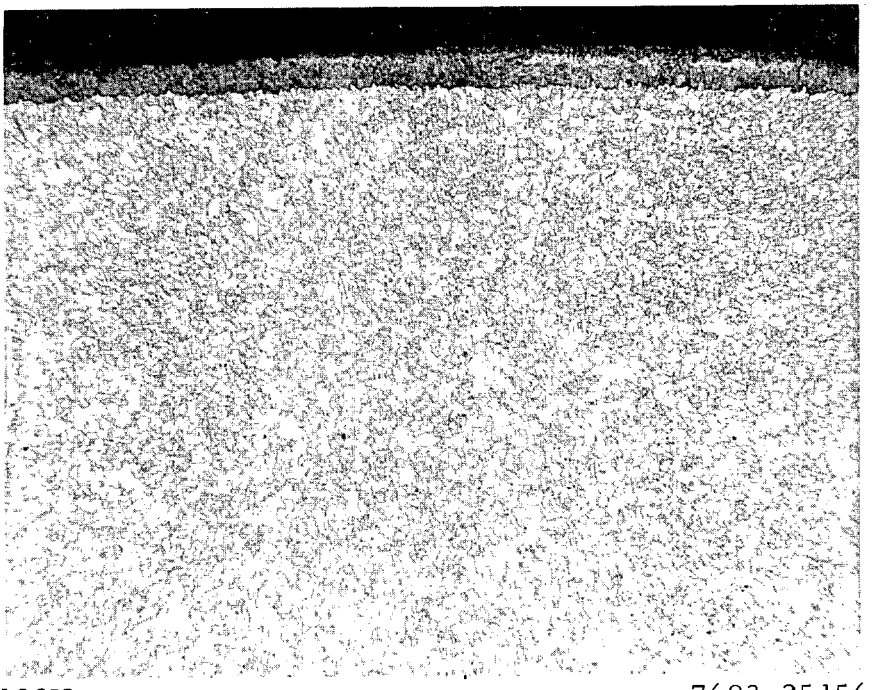

100X 7693-25156

Figure 20. Apparent Corrosion or Depletion Layer (~0.5 mil) on the Tube Outside Diameter of Tube No. 21 (Incoloy 800)

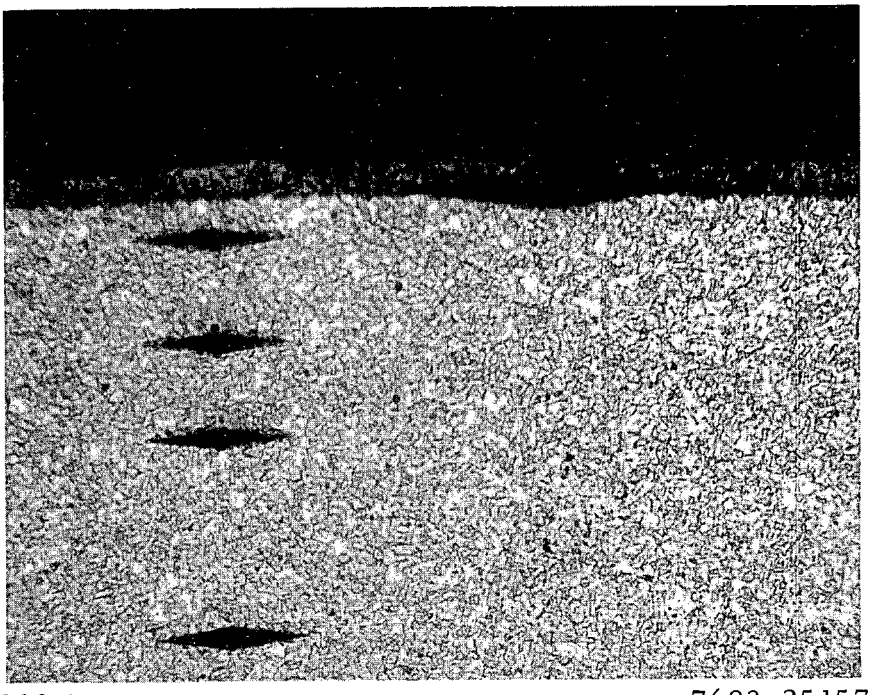

100X 7693-25157

Figure 21. Comparison of the Hardness Indentation on the Depletion Layer and on the Base Material

3. Tube No. 29A (Type 304 SS)

A macrograph of the impact area on tube No. 29A is shown in Figure 22. An indentation (~0.34 x 0.095 x 0.021 in.) was formed on the tube outside diameter. The areas surrounding the indentation appeared to be polished and shiny. Again, no indication of corrosion was observed in the impact area.

Microscopic examination of the impact areas disclosed the following:

1) A partially sensitized structure with no evidence of corrosion in the impact areas (Figure 23).

2) In areas away from the impact, the material exhibited carbide precipitation on grain boundaries, intergranular corrosion, and surface pitting (Figures 24 through 26).

3) A carbide concentration gradient was also found across the tube wall, with the greatest carbide concentration on the tube outside diameter; the absence of carbides on the tube inside diameter is apparent in Figure 27.

4) Some plastic deformation bands were observed on tube outside diameter, as shown in Figure 26.

4. Tube No. 15 (2-1/4 Cr - 1 Mo Ferritic Steel)

Figure 28 is a macrograph of the impacted area on tube No. 15. The size of the impact indentation was 0.07 x 0.082 x 0.012 in.

Metallographic examination of the impact area revealed:

1) A general bainitic structure with large proeutectoid ferritic grains. Examination at high magnification (X1000) disclosed numerous second-phase particles in bainite region and little or no second-phase in the proeutectoid ferrite grains.

2) No indication of corrosion was observed in the impact areas on tube outside diameter.

3) No plastic deformation bands or grain elongation/distortion was observed in grains close to the impact. However, there are some

deformation bands in grains and some elongated grains in areas away from the impact region. These observed indications may be a result of fabrication or handling.

4) A decarburized layer (~3 mils thick) was observed on the outside diameter areas away from the impact; this layer could be attributed to heat-treatment prior to sodium-water-reactions testing.

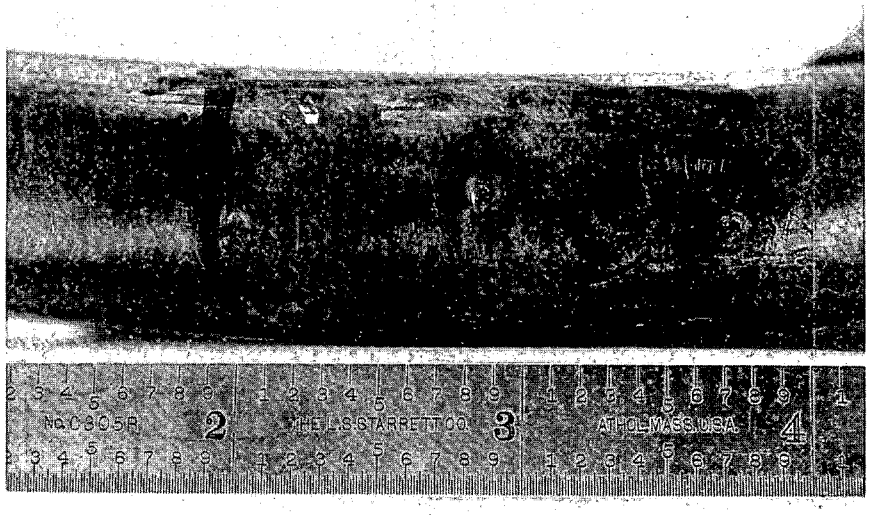

1.5X 7693-25158

Figure 22. Macrograph of the Impact Area on Tube No. 29A (Type 304 SS)

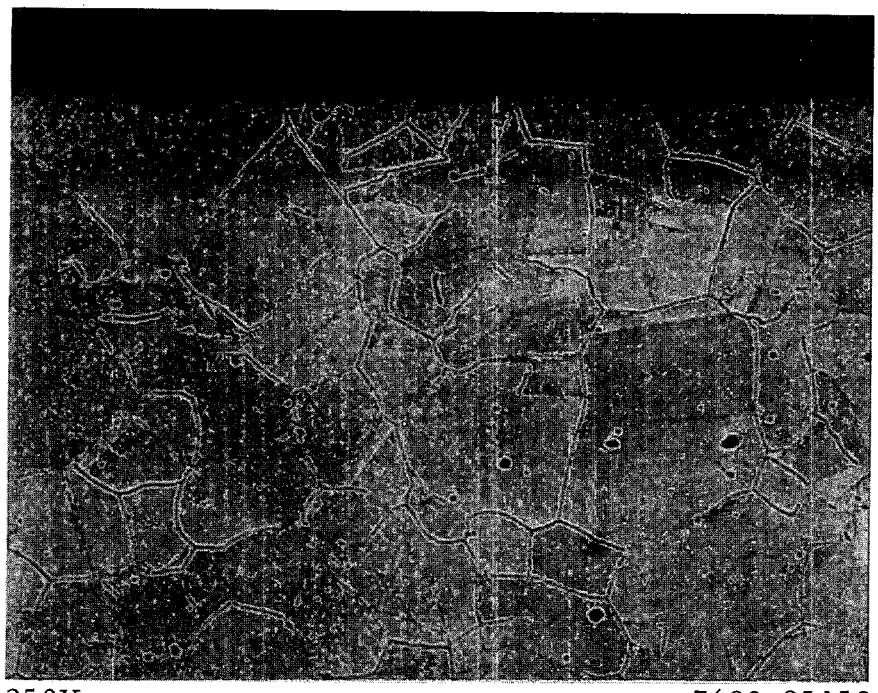

250X 7693-25159

Figure 23. Typical Microstructure of Tube Outside Diameter in Impact Area, Showing Absence of any Corrosion

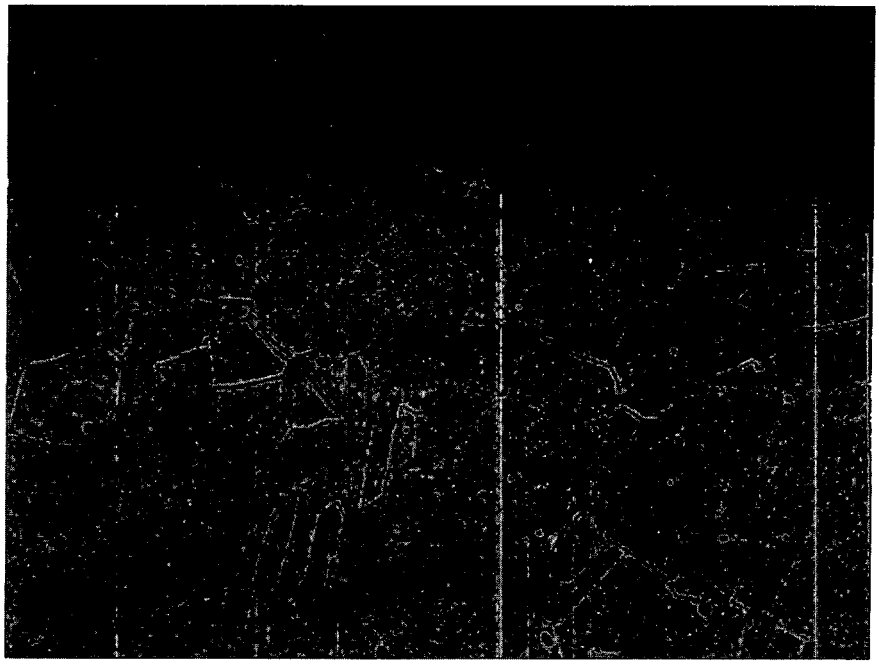

250X 7693-25160

Figure 24. Typical Microstructure of Tube Outside Diameter in Areas Away from Impact, Showing Intergranular Corrosion and Surface Pitting

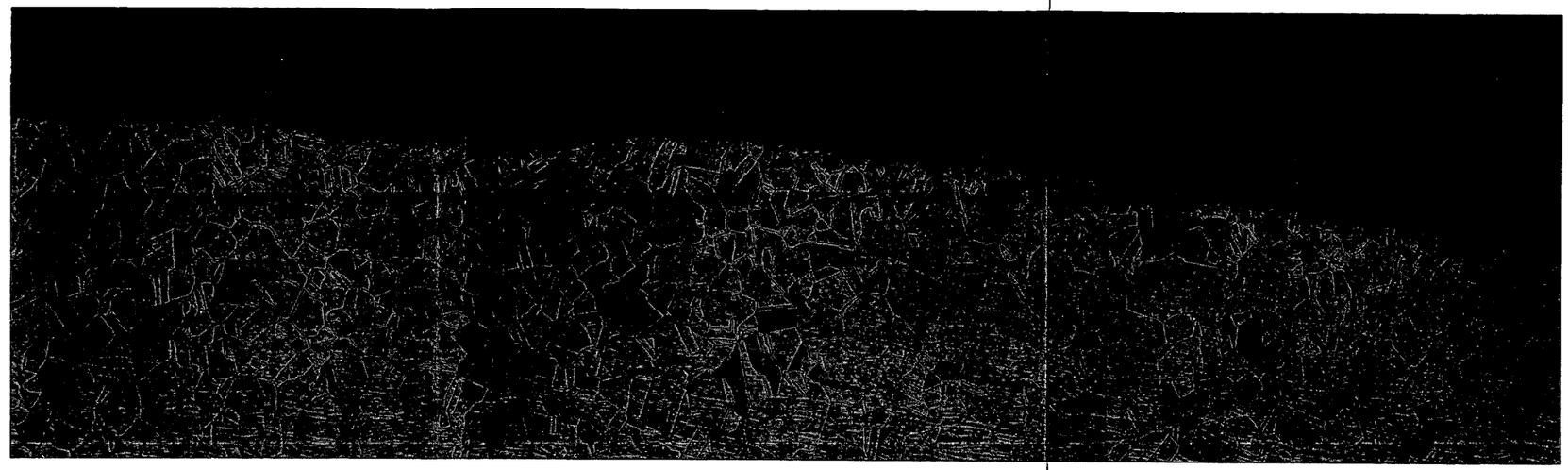

100X 7693-25161

Figure 25. Microstructure of Tube Outside Diameter about 3/4 in. away from the Center of Impact, Showing Corrosion and Plastic Deformation Lines

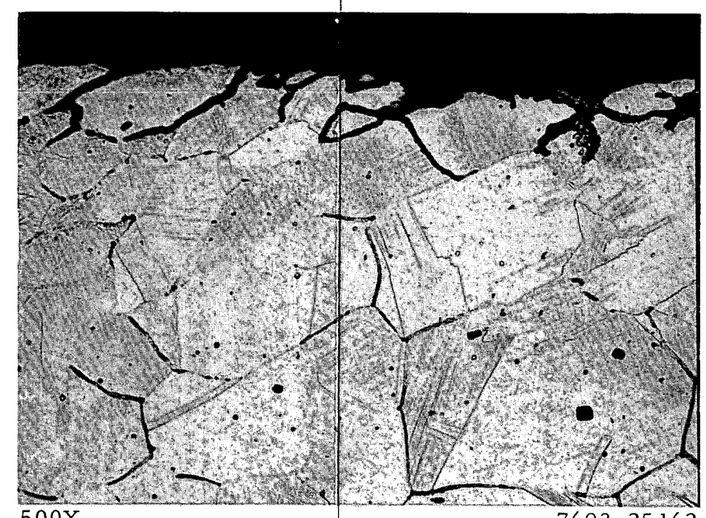

500X 7693-25162

Figure 26. Enlarged View of the Microstructure in the Indented Area, Showing Intergranular Corrosion, Plastic Deformation Lines, and Carbide Precipitation

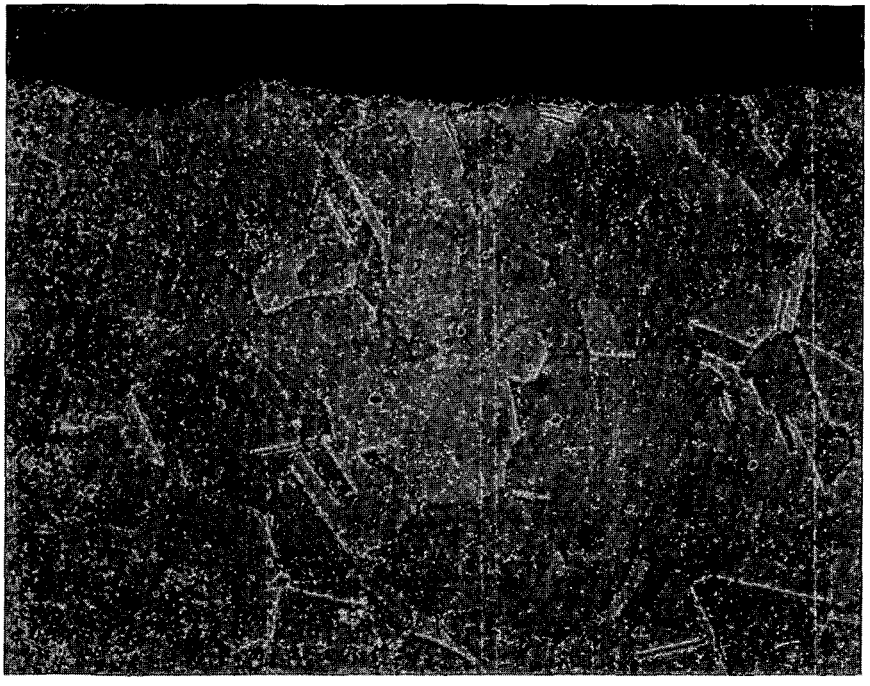

250X

a. Inside Diameter of Tube at Impact Areas

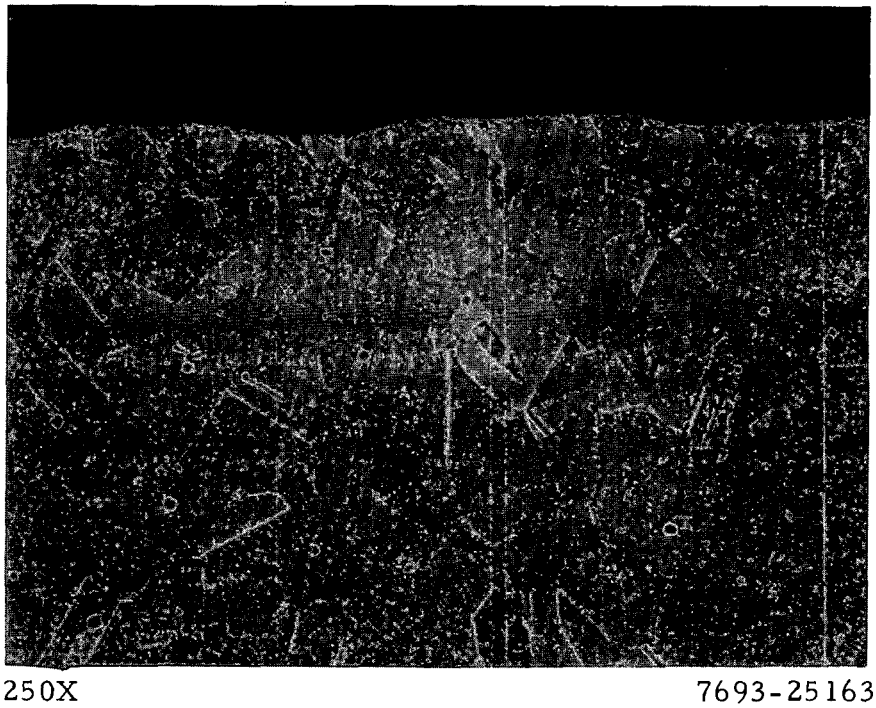

250X 7693-25163

b. Inside Diameter of Tube in Areas Away from Impact

Figure 27. Microstructures of Tube Inside Diameter, Showing the Absence of Carbide Precipitation

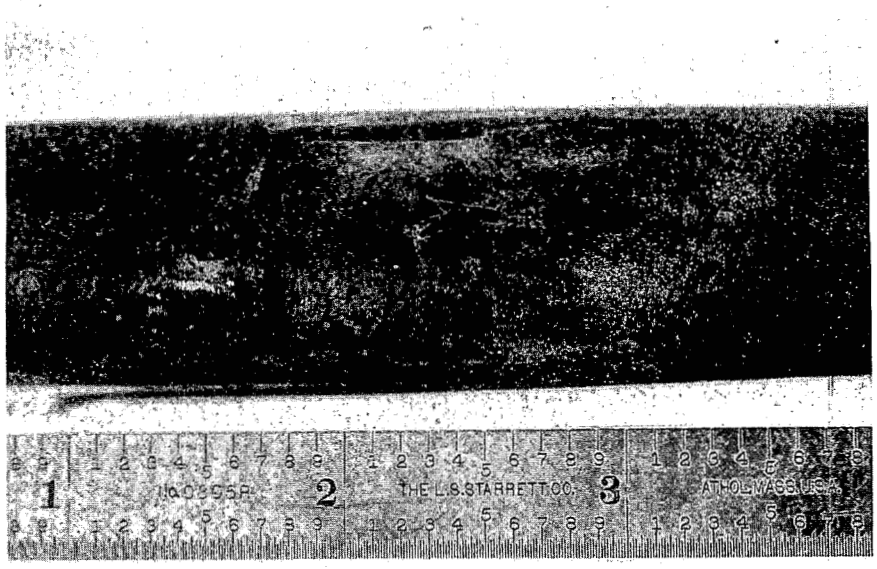

1.5X 7693-25164

Figure 28. Macrograph of the Impact Area on Tube No. 15 (2-1/4 Cr - 1 Mo Steel)

IV. DISCUSSIONS

A. EXTENT OF WASTAGE

The extent of material removal (wastage) due to impact and sodium-water reactions, or both, is presented in Tables 4 and 5. A comparison of the measurements made by LMEC and those made by the Southwest Research Institute (SRI) is shown in Table 6. In general, each of these independent dimensional measurements yielded roughly equivalent material removal results. However, LMEC data and SRI data differed by a maximum of ~30% in the measured volumetric results for tube No. 37.

The average wastage rate data, as presented in Table 6, were obtained by dividing the volume of affected area by the total injection time. This calculation was performed under the assumption that the wastage process occurred primarily during the injection period. This assumption is valid, as substantiated by the available metallographic data which will be discussed in the next section. The average wastage rates of tube No. 15 (2-1/4 Cr - 1 Mo steel), tube No. 21 (Incoloy 800), tube No. 29A (Type 304 SS), and tube No. 37 (2-1/4 Cr - 1 Mo steel) are 0.02×10^{-3} cc/sec, 0.01×10^{-3} cc/sec, 0.15×10^{-3} cc/sec, and 3×10^{-3} cc/sec, respectively. As shown in Table 6, the maximum depths of penetration of tube Nos. 15, 21, 29A, and 37 are 12, 11, 21, and 64 mil, respectively. For tube No. 37, it is important to note that 50% of the tube wall was eroded in only 21 sec. However, it should be additionally noted that tube No. 15 was tested in static sodium. The other three tests were conducted in a dynamic sodium environment with sodium velocity passing the target tubes at about 2 ft/sec.[1] Of the three materials tested in flowing sodium, Incoloy 800 (tube No. 21) exhibited the most resistance to material wastage caused by impact and/or sodium-water reactions. The 2-1/4 Cr - 1 Mo steel (tube No. 37) exhibited the least resistance. Type 304 SS displayed an intermediate wastage rate (0.15×10^{-3} cc/sec) between those of Incoloy 800 and 2-1/4 Cr - 1 Mo ferritic steel. The difference in wastage rate in each case is about one order of magnitude.

The excellent resistance to impact erosion displayed by austenitic stainless steels, with respect to ferritic steel, is probably attributable to their

TABLE 6

COMPARISON OF LMEC AND SRI MEASUREMENTS ON FOUR APDA SODIUM-WATER REACTION TARGET TUBES

Parameters Measured	LMEC Data Tube No.				SRI (APDA) Data Tube No.			
	15	21	29A	37	15	21	29A	37
Maximum Depth, cm (mil)	0.031 (12)	0.028 (11)	0.053 (21)	0.163 (64)	0.031 (12)	0.031 (12)	0.053 (21)	0.160 (63)
Volume of Indentation (cc)	0.002	0.005	0.025	0.060	0.010	0.006	0.027	0.043
Rate of Wastage (cc/sec x 10^{-3})	0.02	0.01	0.15	3	0.08	0.01	0.17	2.2
Injection Duration (sec)(1)	125	570	151	21	125	570	151	21

Note: Tube 15 — 2-1/4 Cr - 1 Mo
Tube 21 — Incoloy 800
Tube 29A — Type 304 SS
Tube 37 — 2-1/4 Cr - 1 Mo

better high-temperature mechanical properties. The ability of the austenitic stainless steels to retain their hot microhardness at high temperatures (T>1200°F) is shown in Figure 29.[3] Although it has higher hardness values at room or low temperatures, relative to Incoloy 800 and Type 304 SS, the drastic reduction of hot hardness for ferritic steel is evident. Figure 30[4-6] is a comparison of the elevated temperature strength of the austenitic stainless steels and ferritic steel. As shown, the decarburized 2-1/4 Cr - 1 Mo ferritic steel is the weakest alloy relative to 2-1/4 Cr - 1 Mo steel and austenitic stainless steels. It is known that erosion resistivity usually increases with increased tensile strength and hardness of the material.[7] Any treatment that will cause an increase of microhardness or tensile strength will, in general, increase erosion resistivity. Conversely, any treatment causing any reduction of microhardness or tensile strength will lead to a decrease of erosion resistivity. Hence, the decarburized layer found in tube Nos. 37 and 15, could also have reduced the general erosion resistivity of the tubes relative to a normal 2-1/4 Cr - 1 Mo steel.

Recent impingement damage data on various materials in liquid metals indicate that the severity of impingement damage may be inversely related to the strain energy of the material.[8] Strain energy is defined as the area beneath the stress-strain curve of a material and can be approximated by the equation:

$$E_{(strain)_T} = \left(\frac{\sigma_y + \sigma_u}{2}\right)_T \epsilon_T$$

where

σ_y = 0.2% offset yield strength of the material at temperature T.

σ_u = tensile strength of the material at temperature T.

ϵ = elongation of the material at temperature T.

As an alternate rough guide for designers, an empirical method is used to correlate wastage rate with readily available material properties. The variation of calculated strain energy with temperature for Incoloy 800, Type 304 SS and 2-1/4 Cr - 1 Mo steel is tabulated in Table 7 and is shown in Figure 31. The excellent impact erosion resistance of Incoloy 800 is again evident, particularly at temperatures above 1400°F.

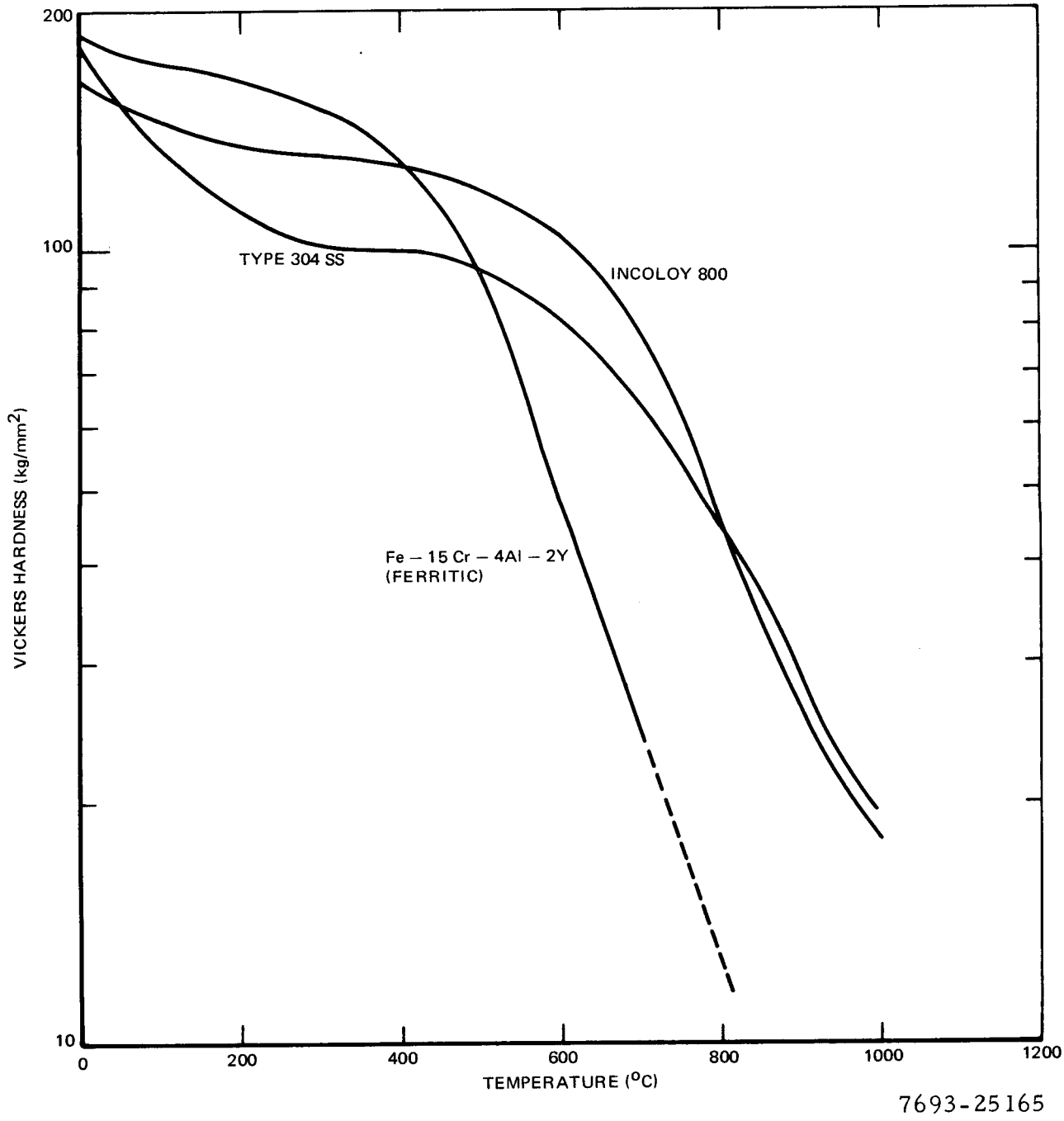

Figure 29. Hot Microhardness Data for Incoloy 800, Type 304 SS, and a Ferritic Steel[3]

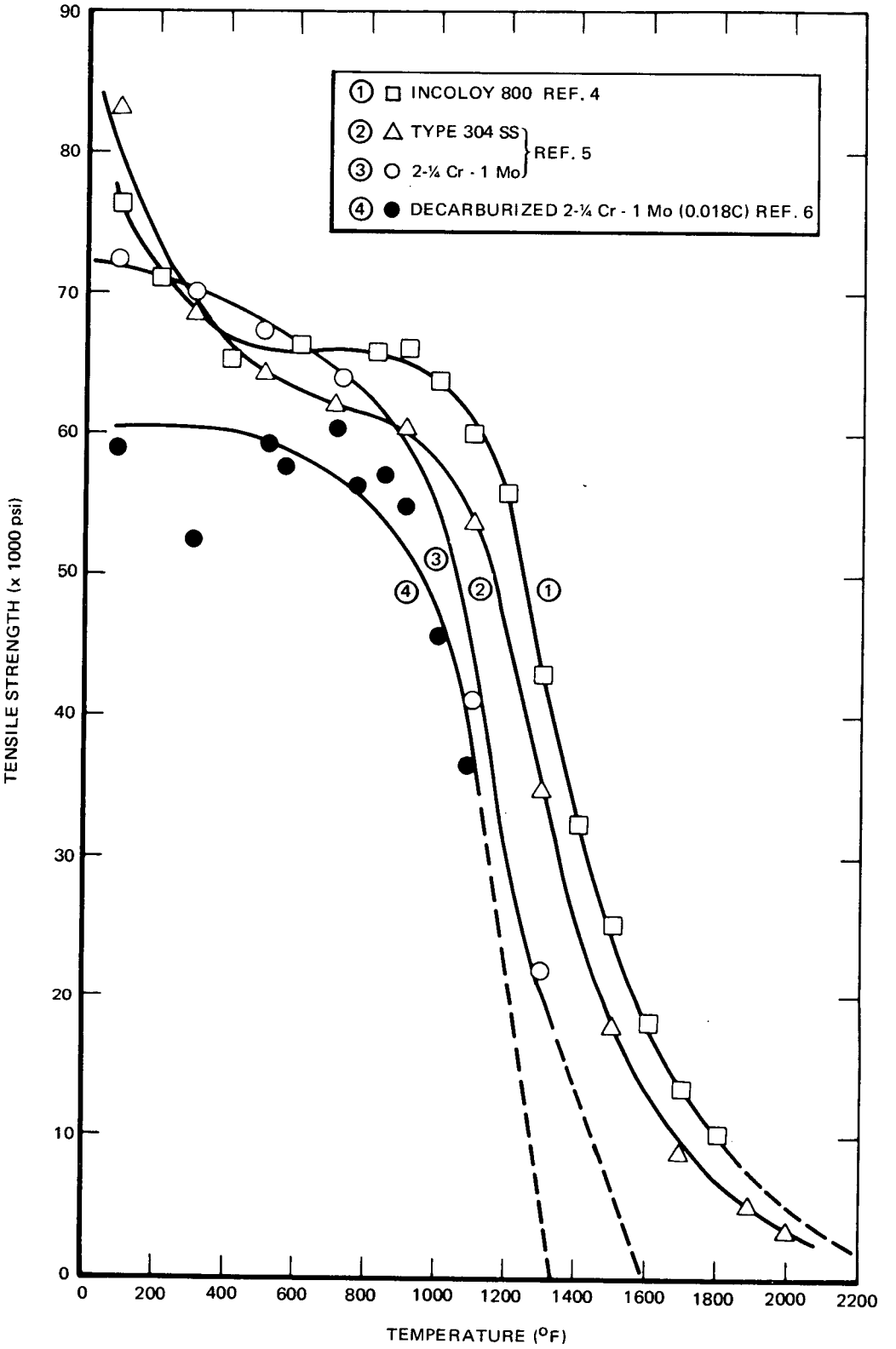

7693-25166

Figure 30. Effect of Temperature on Tensile Strength of Annealed Incoloy 800, Type 304 SS, and 2-1/4 Cr - 1 Mo Ferritic Steel

TABLE 7

VARIATION OF STRAIN ENERGY WITH TEMPERATURE FOR INCOLOY 800, TYPE 304 SS, AND 2-1/4 Cr - 1 Mo STEEL

Temp. (°F)	Incoloy 800*				Type 304 SS†				2-1/4 Cr - 1 Mo Steel†			
	σ_u (psi)	σ_y (0.2% offset) (psi)	ϵ (%)	Strain Energy x 7 x 10^{-2} (kg/mm^2)	σ_u (psi)	σ_y (psi)	ϵ (%)	Strain Energy x 7 x 10^{-2} (kg/mm^2)	σ_u (psi)	σ_y (psi)	ϵ (%)	Strain Energy x 7 x 10^{-2} (kg/mm^2)
80	-	-	-	-	83,000	33,000	64	372	72,000	39,500	33	188
85	76,100	28,200	52.0	270	-	-	-	-	-	-	-	-
200	71,000	24,100	53.0	252	-	-	-	-	-	-	-	-
300	-	-	-	-	68,400	26,400	50	237	70,000	35,800	26	138
400	65,400	21,000	49.5	214	-	-	-	-	-	-	-	-
500	-	-	-	-	64,100	21,800	42	182	67,000	34,500	21	107
600	66,300	17,000	53.0	221	-	-	-	-	-	-	-	-
700	-	-	-	-	61,900	19,500	38	155	64,200	34,000	20	98
800	65,800	18,100	53.0	223	-	-	-	-	-	-	-	-
900	66,000	14,900	56.0	226	60,000	18,100	36	140	60,000	28,000	22	97
1000	63,500	16,500	51.0	204	-	-	-	-	-	-	-	-
1100	60,000	14,200	50.5	187	53,200	16,400	35	122	41,000	16,000	35	100
1200	55,700	14,800	50.0	152	-	-	-	-	-	-	-	-
1300	42,700	14,200	43.0	122	35,000	13,800	35	86	22,000	3,000	60	75
1400	32,300	15,400	78.0	186	-	-	-	-	-	-	-	-
1500	25,200	15,600	96.0	196	18,000	9,900	38	53	-	-	-	-
1600	18,600	11,600	125.0	189	-	-	-	-	-	-	-	-
1700	13,400	9,000	128.0	146	-	-	-	-	-	-	-	-
1800	10,200	8,900	113.0	109	-	-	-	-	-	-	-	-

*The International Nickel Co., Technical Bulletin T-40, "Engineering Properties of Incoloy 800," p 5 (1965)
†Reference 5

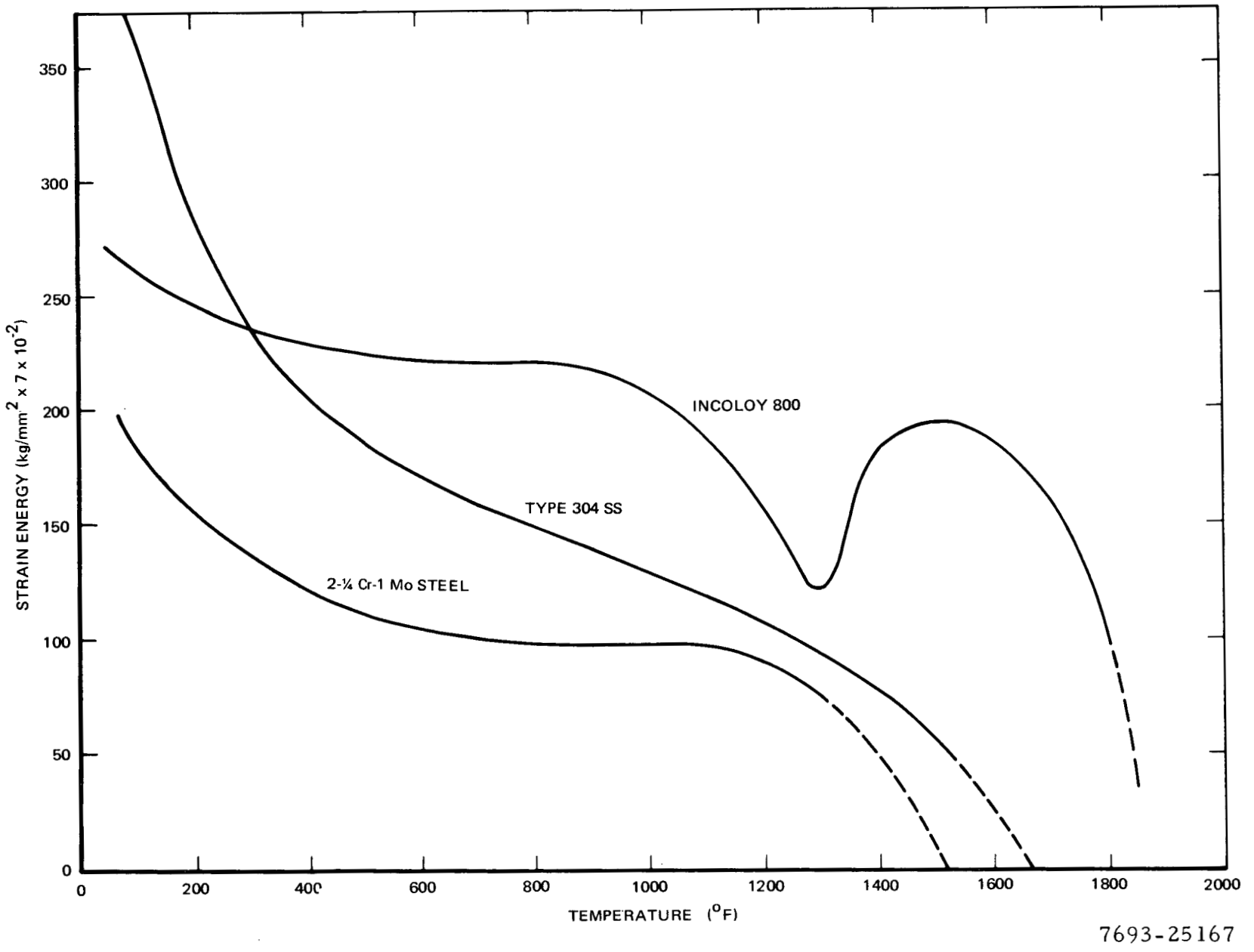

Figure 31. Variation of Calculated Strain Energy with Temperature for Incoloy 800, Type 304 SS, and 2-1/4 Cr - 1 Mo Ferritic Steel

Based on the limited data on average wastage rate of the materials, the dependence of average wastage rate on strain energy of the materials is plotted in Figure 32. At 1500 or 1600°F the variation of average wastage rate with strain energy at the temperatures of the material appears to be linear on a log-log scale (Figure 32). It is noteworthy that this temperature is consistent with the probable maximum temperature obtained from microstructural study (see next section).

Resistance to erosion by cavitation can often be related to ultimate resilience which is defined as:[7]

$$R = \frac{(\sigma_u)^2}{2E}$$

where

σ_u = tensile strength of the material.

E = elastic modulus of the material.

The ultimate resilience for Incoloy 800, Type 304 SS, and 2-1/4 Cr - 1 Mo ferritic steel was calculated and tabulated in Table 8. The variation of ultimate resilience with temperature for Incoloy 800, Type 304 SS and 2-1/4 Cr - 1 Mo ferritic steel is shown in Figure 33. Again, the excellent erosion resistivity of Incoloy 800 with respect to Type 304 SS and 2-1/4 Cr - 1 Mo ferritic steel is apparent.

B. METALLOGRAPHIC ANALYSIS

Compared with the control (quenched) samples, the maximum temperature of the target tubes was estimated to be 1600°F. However, detailed examination at high magnification (~1000X) on the outside diameter of the impact areas for tube Nos. 37 and 15 disclosed the presence of second-phase particles which are similar to the second-phase particles observed in the controlled specimens quenched from 1700 and 1800°F. These second-phase particles were distributed randomly on the outside diameter surfaces. The presence of these second-phase particles, and their distribution, suggest that the local maximum temperature at the outside diameter could conceivably have reached ~1700 and 1800°F.

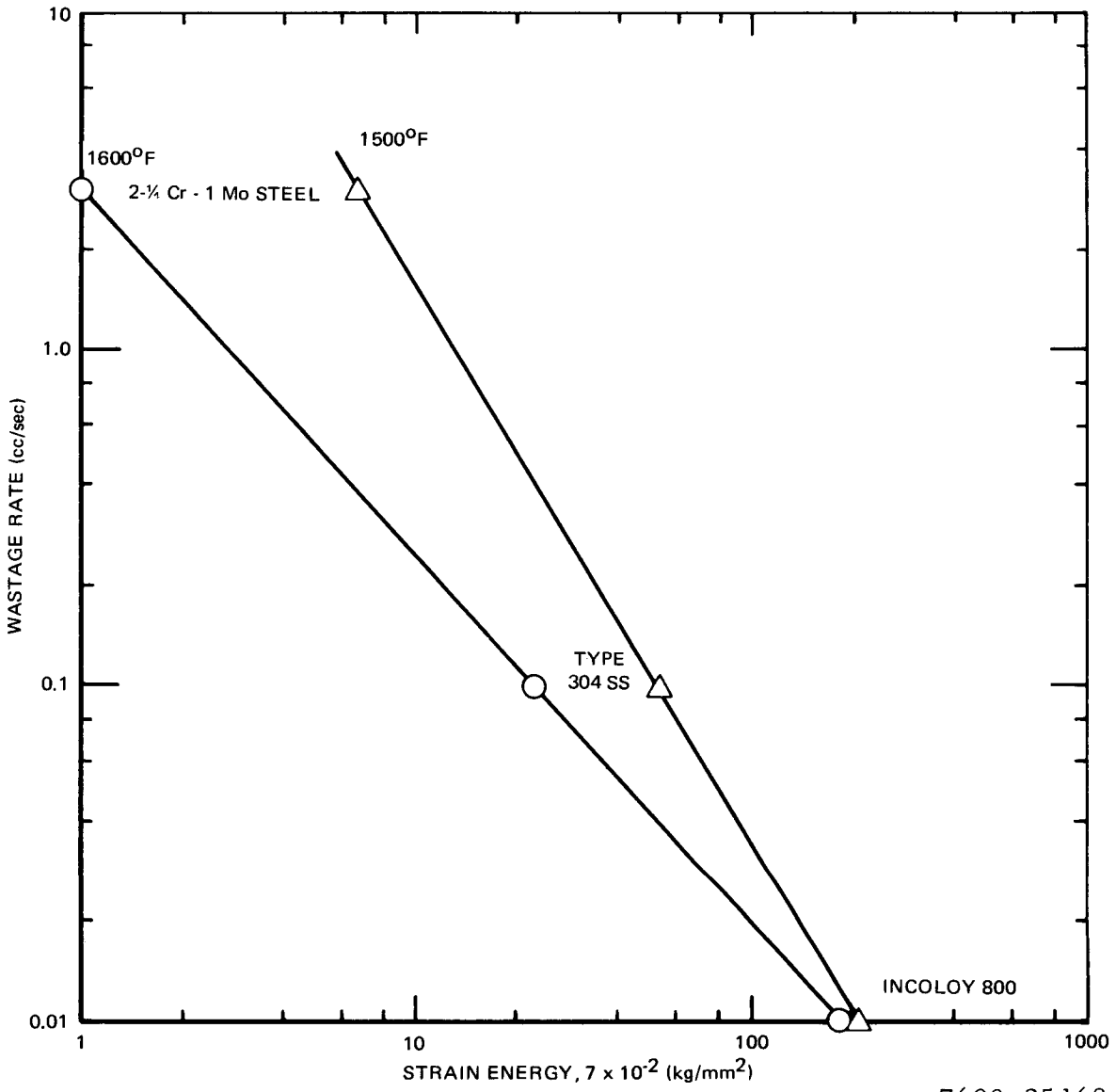

7693-25168

Figure 32. Dependence of Wastage Rate on Strain Energy of Material

TABLE 8

VARIATION OF ULTIMATE RESILIENCE WITH TEMPERATURE FOR INCOLOY 800, TYPE 304 SS, and 2-1/4 Cr - 1 Mo FERRITIC STEEL

Temp. (°F)	Incoloy 800			Type 304 SS			2-1/4 Cr - 1 Mo Ferritic Steel[5]		
	σ_u[4] (psi)	E* (psi x 10^6)	R (in.-lb/in.^{3})	σ_u[5] (psi)	E[9] (psi x 10^6)	R (in.-lb/in.^{3})	σ_u (psi)	E (psi x 10^6)	R (in.-lb/in.^{3})
80	-	-	-	83,000	29.00	119	72,000	29.82	87
85	76,100	10.62	273	-	-	-	-	-	-
100	-	(10.59)	-	-	-	-	-	-	-
200	71,000	10.37	242	-	-	-	-	-	-
300	-	(10.13)	-	68,400	27.40	85.5	70,000	29.10	84
400	65,400	9.91	216	-	-	-	-	-	-
500	-	(9.69)	-	64,100	26.00	79.4	67,000	28.10	80
600	66,300	9.47	232	-	-	-	-	-	-
700	-	(9.25)	-	61,900	25.00	76.8	64,200	26.70	77.5
800	65,800	9.04	241	-	24.00	-	-	-	-
900	66,000	8.82	247	60,000	23.50	76.5	60,000	24.50	73.5
1000	63,500	8.60	235	-	-	-	-	-	-
1100	60,000	8.36	216	53,200	22.30	63.7	41,000	20.40	41.1
1200	55,700	8.12	192	-	-	-	32,000	15.40	32.5
1300	42,700	7.87	117	35,000	21.40	28.6	22,000	-	-
1400	32,300	7.58	59	-	-	-	-	-	-
1500	25,200	7.25	44	18,000	20.00	8.1	-	-	-
1600	18,600	6.82	25	-	-	-	-	-	-
1700	13,400	-	-	-	-	-	-	-	-
1800	10,200	-	-	-	-	-	-	-	-

*Young's Modulus of Elasticity

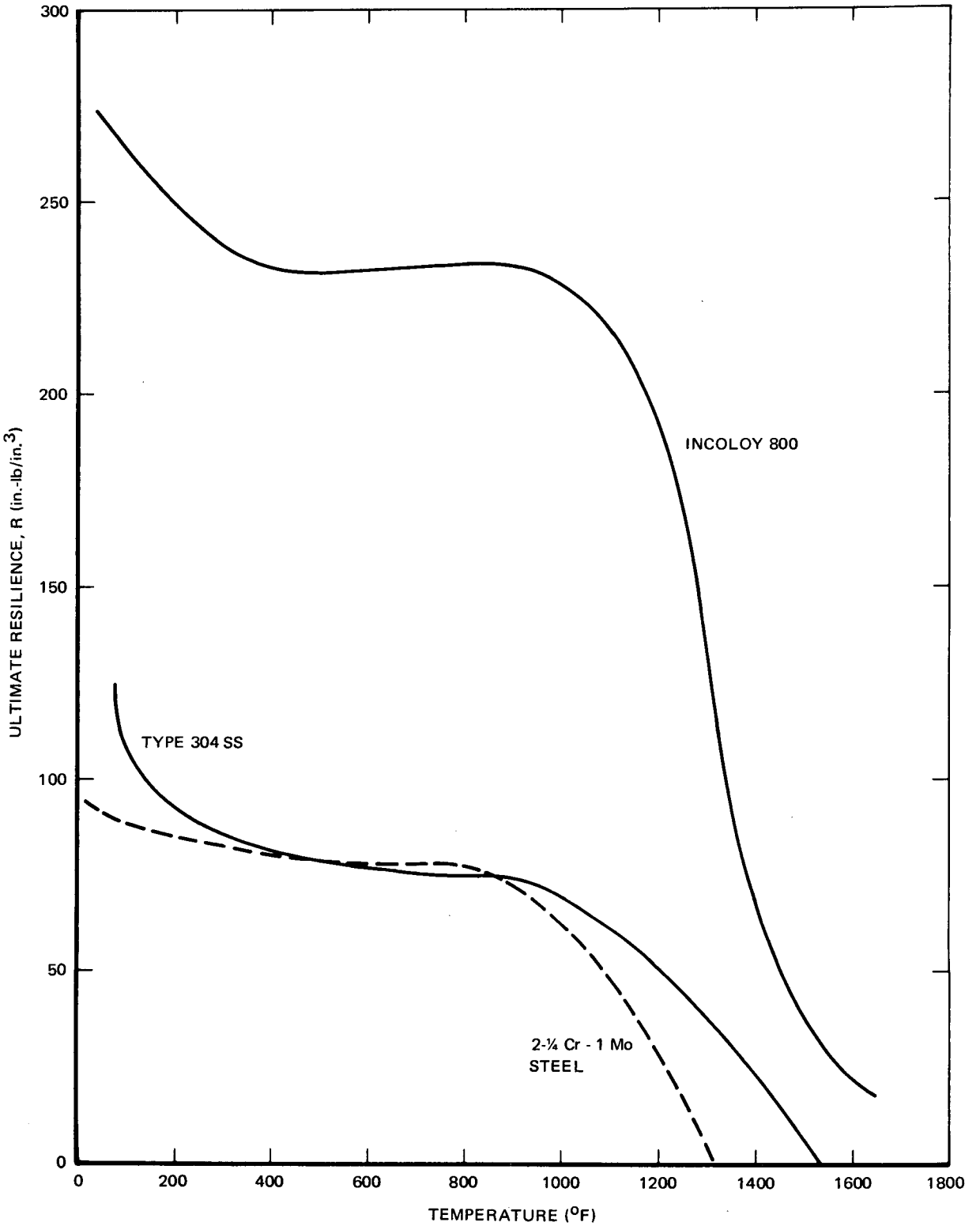

7693-25169

Figure 33. Variation of Ultimate Resilience with Temperature for Incoloy 800, Type 304 SS, and 2-1/4 Cr - 1 Mo Ferritic Steel

For tube No. 21 (Figure 17), dense carbide precipitation was observed on grain boundaries and twin boundaries at the outside diameter, a microstructure typical of sensitized Incoloy 800. This dense carbide precipitation occurred only within one-third of the tube wall (i.e., ~1/24 in. thick) on the tube outside diameter. Areas adjacent to the tube inside diameter (covering about two-thirds of the tube wall) exhibited a cold-worked microstructure with longitudinal plastic flow lines resulting from fabrication. In these areas, carbide precipitation is nearly absent. This observed carbide precipitation gradient across the tube wall suggests the presence of a large thermal gradient (minimum ΔT = 700°F and maximum = 1000°F) across the tube wall with the maximum temperature at the tube outside diameter. With a water injection time of 570 sec and the presence of carbides on twin boundaries, the maximum temperature could be as high as 1900°F (Figure 34). But when compared to the control sample and the absence of grain growth in impact areas, this maximum temperature would be only 1500°F. Incorporating this data with the microstructural and hardness data obtained for Type 304 SS and 2-1/4 Cr - 1 Mo steel, it is concluded, therefore, that the maximum temperature the target tubes reached was 1600°F. The estimation is probably within ±100°F.

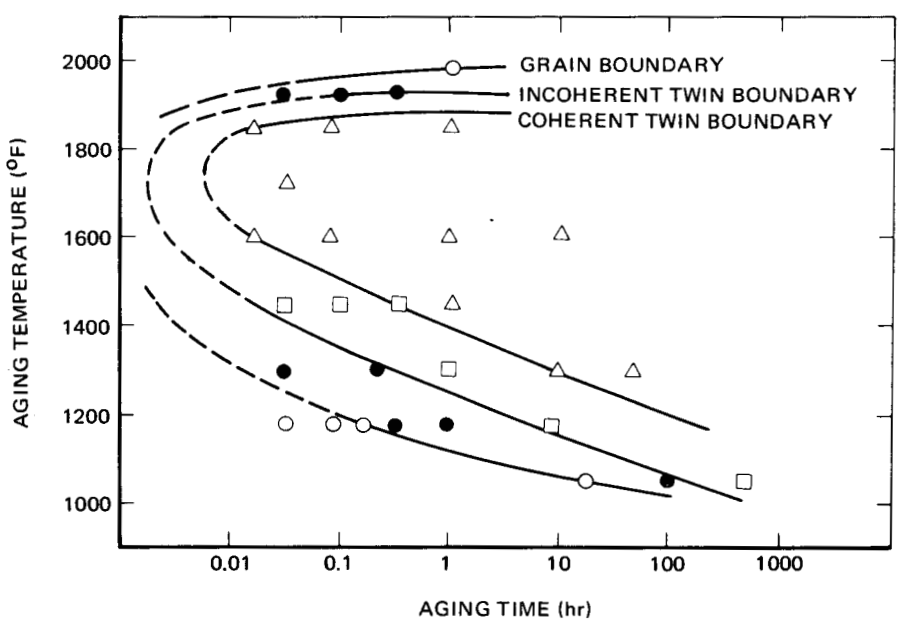

7693-25170

Figure 34. Time-Temperature Dependence of $Cr_{23}C_6$ Precipitation in Incoloy 800 with 0.07% C[10]

An attempt was made to chart the temperature profile in the impact area of all the target tubes. But the change in microstructure and hardness values was not sufficient to yield meaningful results. Furthermore, the decarburization on the outside diameter of tube Nos. 15 and 37 complicated and reduced the reliability of the temperature estimation.

It is also interesting to note the grain boundary carbide distribution in the austenitic stainless steel target tubes (Nos. 21 and 29A). Grain boundary carbides were found across the tube wall at and around the impact area. In other areas, only a thin layer of grain boundary carbides was faintly visible on the tube outside diameter; no grain boundary carbide was found on the inside diameter away from impact. These observations suggest that the temperature rise due to sodium reaction was the highest at or around the impact area. It decreased with distance from impact.

It is significant that light microscopy, because of limited resolution, can give only a limited estimation of the maximum temperature. Since carbide precipitation (and morphology) is a temperature- and time-dependent process, more accurate temperature estimation may be obtainable by electron microscopy. In addition, election microscopy can yield a more accurate and reliable result on strain deformation due to impact. It is recommended, therefore, that electron microscopy be utilized to analyze any future target tubes.

C. NATURE OF DAMAGE CAUSED BY WATER-JET IMPACT AND SODIUM-WATER REACTION

For all the target tubes examined, it is a very significant finding that there was no evidence of corrosion in the indented impact areas. For tube No. 21 (Incoloy 800) and tube No. 29A (Type 304 SS), there were minor indications of intergranular corrosion and transgranular pitting only in areas away from impact. These minor corrosion indications are probably attributed to corrosion by sodium-water reaction products. The absence of corrosion in the indented impact area substantiates the conclusion that the material removal process was controlled primarily by impingement or erosion. The apparent flow pattern (like a river delta) produced by erosion/impingement is shown in Figure 11.

Deformation bands and some elongated grains were observed on the outside diameter of the four target tubes, particularly those of Type 304 SS and of

Incoloy 800; however, their distribution appears to be random on the outside diameter of the four tubes. Therefore, the origin of some of the deformation lines in the impact areas can not be positively identified as a result of plastic straining caused by temperature surge, which resulted from the violent exothermic sodium-water reactions. The observed deformation bands and elongated grains could also have been introduced during fabrication. This absence of any dominant and reliable indication of plastic deformation in the indented impact areas suggests that the deformation lines could have been annealed (healed) by the high temperature generated in the impact zone.

D. POSSIBLE WASTAGE MECHANISM

In general, impingement erosion is a plastic deformation process which increases the tensile strength and microhardness of work hardenable materials, such as Incoloy 800 and Type 304 SS. The absence of any dominant plastic deformation lines and of corrosion at the impact area suggests that the wastage process could have occurred in a high-temperature environment which annealed out (healed) the plastic deformation bands. In this regard, the wastage process in sodium-water reactions appears to be analogous to a high quality thermal-arc plasma cutting/hole-piercing process in which the plasma arc rapidly penetrates through the material, forming a hole/indentation about equal to the diameter of the plasma arc stream. In the APDA tests, the stream would contain a jet of water and/or sodium-water reaction products traveling at high velocity (and at high temperatures) impinging on the target material. Material removal would then be controlled by the temperature and flow velocity of the jet (stream) of steam and/or sodium-water reaction products. This mechanism of wastage, due to sodium-water reactions, differs from the material removal process, due to rain-drop impingement/cavitation, primarily in the temperature at which the process occurs. In sodium-water reaction, the surge in temperature due to the exothermic reactions will enhance the wastage process, since the material will be weaker (and softer) at higher temperatures.

E. OTHER FACTORS AFFECTING WASTAGE RATE

The effect of high-temperature mechanical properties (e.g., tensile strength, ductility, etc.) on erosion resistivity was discussed previously. In addition,

there are many other parameters which influence the wastage rate of a target material. These primary parameters can be categorized into two main groups: (1) test conditions/environments, such as the velocity of the water-jet or leak rate, leak duration, size and shape of leak orifice, spacing between the leak and target (material), orientation of water-jet relative to target tube (i.e., the angle of incidence), target tube material temperature, sodium temperature, sodium velocity, and background pressure in the reaction chamber; and (2) the target material and its condition, such as the metallurgical conditions of the material (i.e., annealed or cold-worked), the grain size, the surface finish or roughness, and its fabrication and thermal histories.

For the tests reported here, the orientation of the water-jet relative to the target tube is of particular concern because of its uncertainty in control. It is known that the normal component of impact velocity is of paramount significance in determining erosion/impingement damage.[11] Baker et al., related the rate of mass loss due to impingement to impact velocity, and the angle of incidence (θ) by the following equation:[11]

$$\left(\frac{\delta M}{2\omega}\right) = K\,(V \sin\theta - V_c)^n \operatorname{Cosec}\theta$$

where K, V_c, and n are material constants, and V is the velocity of the water-jet. From the orientation of the indentation relative to the centerline of the target tube, the angle of incidence apparently was not constant in all the tests. This variation could have added to the large data scatter usually found in sodium-water reactions tests. In addition, the injection rate, injection duration, and the injection orifice size were not exactly identical for each of the four tests (Table 2). They would undoubtedly contribute to the uncertainties in the reported wastage rates.

It is noteworthy also that the target tube materials were not characterized sufficiently to yield a clear-cut conclusion with respect to the wastage results. As mentioned earlier, under constant test conditions, the wastage rate is influenced by test material conditions (anneal or cold work material), grain size, second-phase precipitation, and surface roughness or finish. Material wastage by erosion/impingement can be considered as a mechanical deformation process

in which strong local stresses can be formed due to impact within the metal, or that considerable localized deformations can occur, giving rise to material wastage/indentation. Since both of these effects/processes are related to moving dislocations, it is necessary to decrease their (dislocations) mobility in order to minimize damage by suitable dislocation obstacles. These obstacles can be precipitates (e.g., carbide and sigma particles), grain boundaries, other dislocations (e.g., cold-work), and other defects.

It is recognized that precipitation of particles of optimum spatial distribution and of optimum size can cause an increase of tensile strength and of microhardness by hindering dislocation movement. This increase of tensile strength and of microhardness can, in turn, increase erosion resistivity. This behavior has been observed for many age-hardenable materials, dispersion-hardened metals, work-hardenable alloys, and carburized and nitrided steels.[12]

Investigations of the influence of grain boundaries on erosion resistivity of metals have been conducted by Hoff, Langbein, and Rieger.[12] It was observed that the erosion resistivity increases with decreasing grain size. Among the three materials tested (Incoloy 800, Type 304 SS, and 2-1/4 Cr - 1 Mo ferritic steel), Incoloy 800 displayed the smallest grain size (finer than ASTM No. 8) relative to the other two materials (ASTM No. 2 for Type 304 SS and ASTM No. 7 for 2-1/4 Cr - 1 Mo). However, the extent of grain size effect on the wastage rates of material cannot be defined in this particular test.

The four target tubes also exhibited some degree of cold-work, which increases the yield strengths of work-hardenable alloys, such as Incoloy 800 and Type 304 SS. Cold work does not significantly influence the mechanical properties of ferritic steels (e.g., 2-1/4 Cr - 1 Mo steel). This cold work is related to material deformation which, in turn, is connected with dislocations and their interactions. Depending on their mechanical stress field, the dislocations interact with each other. Moreover, depending on the signs of the Burger's vectors and the orientation of slip planes, dislocations can annihilate each other upon combination if their Burger's vectors are of opposite signs. If the dislocations are of similar signs, they will repel each other at an equilibrium distance, thus setting up an internal stress field which can increase the hardness of the alloy.

In the case of dislocation combination, the resultant new dislocation will be immobile if it lies in a nonslip plane. This immobile dislocation would serve as a barrier to movement of other dislocations (thus deformation). This dislocation interaction characteristic, acting as a dislocation obstacle to itself, also results in increased erosion resistivity. For instance, tests show that the incubation time for wastage of cold-worked copper specimens is approximately 25% greater than the incubation time for wastage of annealed copper specimens.[12] These test results show that erosion resistivity can be increased by means of homogeneous deformation of a strain-hardenable metal or alloy. Since both Incoloy 800 and Type 304 SS are strain-hardenable alloys, the contribution of cold work to lowering the wastage rates of both austenitic stainless steels, is real but its extent is uncertain. However, it is clear that this contribution could have increased the erosion resistance of Incoloy 800 and Type 304 SS but could not have as great an effect on 2-1/4 Cr - 1 Mo ferritic steel.

The surface conditions which may affect the resistance of the material against erosion may include conditions of prestress, the degree and extent of work hardening, the prevalence of surface or immediate subsurface flaws which can act as stress raisers and crack-initiation points, and the manner in which the surface geometry facilitates local stress patterns conducive to rapid formation of detached fragments. The target tubes examined exhibited different surface-finish conditions, which again may affect the wastage rates obtained for the material.

In view of the aforementioned discussion of various parameters on wastage/erosion, the importance of controlled metallurgical variables can not be overemphasized for accurate and reliable interpretation of the wastage data.

V. CONCLUSIONS

Based on the volumetric measurements and metallographic data from four APDA small leak sodium-water reaction target tubes, it can be concluded that:

1) Material loss (wastage) resulted primarily from water-jet impact (or erosion). No evidence of corrosion was found in the impact areas. Tube surface temperature rise due to sodium-water reactions enhanced the wastage process in all the target tubes. For tube Nos. 37 and 15 (both were 2-1/4 Cr - 1 Mo ferritic steel), the presence of surface decarburization also reduced the general erosion resistivity of the material.

2) Among the three materials tested in flowing sodium, Incoloy 800 (tube No. 21) exhibited the most resistance and 2-1/4 Cr - 1 Mo ferritic steel displayed the least resistance. The average wastage rates obtained are 1×10^{-5} cc/sec, 1.5×10^{-4} cc/sec, and 3×10^{-3} cc/sec for tube No. 21 (Incoloy 800), tube No. 29A (Type 304 SS), and tube No. 37 (2-1/4 Cr - 1 Mo), respectively. The maximum depths of wastage for tube Nos. 37, 29A, and 21 were 64 mil (in 21 sec), 21 mil (in 151 sec) and 11 mil (in 570 sec), respectively. Tube No. 15 (2-1/4 Cr - 1 Mo) was tested in static sodium and exhibited a wastage rate of 2×10^{-5} cc/sec (maximum depth of penetration: 12 mil in 125 sec).

3) For the austenitic stainless steels tested (Incoloy 800 and Type 304 SS), the presence of minor intergranular corrosion in tube surfaces away from impact, and of a corrosion/depletion layer on the Incoloy 800 tube outside diameter suggest that the wastage process may also have been influenced by corrosion. These corrosion indications, however, were not found on ferritic steel samples.

4) A maximum temperature of 1600°F (±100°F) was estimated for the target tubes. There is, however, an indication that a somewhat higher temperature (~1700 to 1800°F) may have been attained on a very thin surface layer of tube No. 37 (in the impact area).

5) Surface grain elongation and plastic deformation lines were observed in the areas of impact for the target tubes, which suggests the presence of localized deformation, possibly caused by impact/impingment. But on a number of occasions, deformation lines and elongated grains, which were probably a result of fabrication/handling, were also found in areas away from impact. Therefore, without the knowledge of the tube microstructures before sodium-water reaction tests or of archive samples, the cause(s) for the surface grain elongation and deformation cannot be ascertained.

REFERENCES

1. H. V. Chamberlain, J. H. Coleman, E. C. Kovacic, and A. S. Shoudy, "Wastage of Steam Generator Materials by Sodium-Water Reactions," Proceedings of the International Conference on Sodium Technology and Fast Reactor Design, November 7-9, 1968, ANL-7520, Part I, pp 384-409

2. "Properties and Selection," Metals Handbook, American Society for Metals, Volume 1 (1961)

3. J. L. Kamphouse, D. A. Myers, and J. Moteff," Hot-Microhardness Values for Metals and Alloys," GEMP-716 (December 1969)

4. "Engineering Properties of Incoloy 800," The International Nickel Co. Technical Bulletin T-40, (1965)

5. "Steels for Elevated Temperature Service," U. S. S. Bulletin ADUSS 43-1089 (1966)

6. B&W Prototype Steam Generator Development Program Progress Report, July-August 1969

7. J. M. Hobbs, "Experience with a 20-KC Cavitation Erosion Test," Symposium on Erosion by Cavitation or Impingement, ASTM-STP408 (1966)

8. S. G. Young and J. R. Johnson, "Accelerated Cavitation Damage of Steels and Superalloys in Sodium and Mercury," Symposium on Erosion by Cavitation or Impingement, ASTM-STP408 (1966)

9. J. A. De Mastry and M. Kangilaski, "Mechanical and Physical Properties of Fuels and Cladding Materials with Potential for use in Fast Reactor," BMI-X-455, Part 1 (1968)

10. C. N. Spalaris, "Incoloy 800 for Nuclear Fuel Sheaths," GEAP-4633 (July 1964)

11. D. W. Baker, K. H. Jolliffe, and D. Pearson, "The Resistance of Materials to Impact Erosion Damage," Royal Soc. of London, Philosophical Trans. 260 (No. 1110), p 193 (July 1966)

12. G. Hoff, G. Langbein, and H. Rieger, "Material Destruction Due to Liquid Impact," Symposium on Erosion by Cavitation and Impingement, ASTM-STP408 (1966)